The 9.355 GHz Complex Permittivity of Light and Heavy Water from 1 to 90 °C Using an Improved High-Precision Instrumentation System

Xiping Hu,† Harvey A. Buckmaster,*,‡ and Oscar Barajas

Department of Physics and Astronomy, The University of Calgary, Calgary, Alberta, Canada T2N 1N4

Recent improvements to a high-precision instrumentation system for measuring the complex permittivity of high loss liquids using a variable-length transmission sample cell at microwave frequencies are described. An error analysis for this system is given. These improvements have enabled the complex permittivity of heavy water and of double-distilled, deionized light water to be measured with a typical accuracy of ±0.1% for ϵ' and ±0.2% for ϵ'' and a precision of about 0.02% at 9.355 GHz in the temperature interval from approximately 1 to 90 °C in increments of about 2.5 °C. The values of $\epsilon'(t)$ and $\epsilon''(t)$ have been fitted to empirical quintic polynomials in the temperature t (°C). For light water $\epsilon'(t) = 44.628(3) + (13.929(8) \times 10^{-1})t - (3.222(6) \times 10^{-2})t^2 + (3.165(17) \times 10^{-4})t^3 - (1.503(21) \times 10^{-6})t^4 + (2.67(9) \times 10^{-9})t^5$ and $\epsilon''(t) = 40.573(3) - (1.475(6) \times 10^{-1})t - (2.477(4) \times 10^{-2})t^2 + (6.092(12) \times 10^{-4})t^3 - (6.000(15) \times 10^{-6})t^4 + (2.213(7) \times 10^{-8})t^5$ and for heavy water $\epsilon'(t) = 31.452(17) + (16.630(28) \times 10^{-1})t - (2.796(17) \times 10^{-2})t^2 + (1.141(45) \times 10^{-4})t^3 + (0.920(54) \times 10^{-6})t^4 - (7.16(23) \times 10^{-9})t^5$ and $\epsilon''(t) = 37.610(9) + (4.952(16) \times 10^{-1})t - (4.749(10) \times 10^{-2})t^2 + (9.659(26) \times 10^{-4})t^3 - (8.609(30) \times 10^{-6})t^4 + (2.913(13) \times 10^{-8})t^5$. The temperature dependences of the Gibbs free energy, enthalpy, and entropy of activation parameters for the relaxation process as well as the relaxation time have been calculated from both the $\epsilon'(t)$ and $\epsilon''(t)$ data sets for both light and heavy water.

Introduction

The complex permittivity of high loss liquids has been studied extensively by many researchers over the past 50 years. These studies have been summarized by Hasted (*1*) and Buckmaster (*2*). The latter surveyed the evolution of the instrumentation techniques used to make these measurements. During the past decade, Buckmaster and his co-workers (*3*–*12*) have developed a method by which the complex permittivity of high loss liquids can be measured both accurately and precisely using a variable-length transmission sample cell and a dual-channel, double superheterodyne signal processing system. Their initial objective was to improve the precision of such measurements and later to improve their accuracy by implementing improvements to this instrumentation system. The experiments were performed at a single frequency but over a wide temperature range. McAvoy and Buckmaster (*3*) reported 9.346 GHz complex permittivity measurements on water at 20 and 25 °C. Subsequently, Zaghloul and Buckmaster (*6*) extended these measurements at 9.356 GHz to the temperature interval from 10 to 40 °C, and van Kalleveen and Buckmaster (*8*) studied the temperature interval from approximately 1 to 10 °C. Recently Barajas and Buckmaster (*11*) have reported the first determination of the complex permittivity of water at 9.355 GHz in the temperature interval from approximately 1 to 90 °C in increments of about 2 °C. However, a nonlinear fit of their data to the Cole–Cole equation (*13*) to calculate the activation parameters for the relaxation process in small temperature intervals indicated that the ϵ'' data below approximately 10 °C and the ϵ' data above approximately 60 °C had a poorer accuracy since the values of these parameters obtained from the $\epsilon'(t)$ and $\epsilon''(t)$ data sets did not agree. They suggested that the calculated values of these parameters could be used as a diagnostic test for instrumentation deficiencies. They concluded that sample cell thermal gradients below 10 °C and sample vapor bubbles above 60 °C were probably responsible for these discrepancies.

This paper describes recent improvements to this 9.355 GHz instrumentation system and gives an analysis of the error factors. It also reports a new set of 9.355 GHz complex permittivity measurements on both heavy water and double-distilled, deionized light water in 2.5 °C increments for the temperature interval from approximately 1 to 90 °C. The activation parameters for the relaxation process and the relaxation times have been calculated independently from the $\epsilon'(t)$ and $\epsilon''(t)$ data sets for each liquid. The values for light water are compared with those reported by Barajas and Buckmaster (*11*). This paper reports the first comprehensive high-precision, variable-temperature microwave complex permittivity study of heavy water and extends the pioneering measurements of Collie et al. (*14*) and others (*1*).

Measurement Principles

Microwave power is transmitted through the liquid under study when the complex permittivity is measured using a variable-length transmission sample cell as shown in Figure 1. The sample cell length is varied in small increments of length z over a predetermined sample cell length interval. When the moveable waveguide portion of the sample cell is set to the initial position, the voltage at the reference plane (the increment step number is zero) is

$$v_0 = A_0 e^{j\phi_0} \tag{1}$$

where A_0 is the magnitude and ϕ_0 is the phase of V_0. The signal at the plane of increment step number n is

* To whom correspondence should be addressed.
† Permanent address: RF and Microwave Division, The National Institute of Metrology, Beijing 100013, People's Republic of China.
‡ Present address: Department of Electrical and Computer Engineering, University of Victoria, P.O. Box 3055, Victoria, British Columbia, Canada V8W 3P6.

0021-9568/94/1739-0625$04.50/0

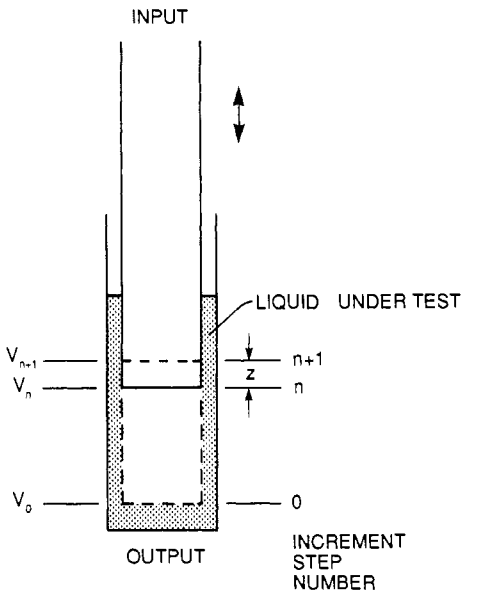

Figure 1. Conceptual diagram for a variable-length transmission sample cell.

$$v_n = A_n e^{j\phi_n} = v_0 e^{-(\alpha+j\beta)nz} \quad (2)$$

where A_n is the magnitude and ϕ_n is the phase of V_n. At the plane of the next increment step number $(n + 1)$

$$v_{n+1} = A_{n+1} e^{j\phi_{n+1}} = v_0 e^{-(\alpha+j\beta)(n+1)z} \quad (3)$$

It follows from eqs 2 and 3 that

$$\alpha = \ln[A_n/A_{n+1}]/z \quad (4a)$$

and

$$\beta = (\phi_n - \phi_{n+1})/z \quad (4b)$$

where α and β are the attenuation and phase shift coefficients, respectively, of the measured sample liquid. Equations 4a and 4b are the responses under ideal measurement conditions. The amplitude and phase of the signal are measured and recorded at each increment step. It follows that a set of α and β values which correspond to each increment step can be calculated. These values of α and β should ideally have the same value for a fixed value of z independent of the choice of reference plane. The complex permittivity, $\epsilon = \epsilon' - j\epsilon''$, where ϵ' is the permittivity and ϵ'' is the dielectric loss, can be calculated from α and β using the following equations (*1*):

$$\epsilon' = [\lambda/2\pi]^2(\beta^2 - \alpha^2) + [\lambda/\lambda_c]^2 \quad (5a)$$

$$\epsilon'' = [\lambda/2\pi]^2 2\alpha\beta \quad (5b)$$

where λ is the free-space wavelength and λ_c is the cutoff wavelength for the sample cell. An incremental differential diagram for either α and β can be created by plotting successive values of these parameters as a function of the incremental step number. These graphs would be straight lines with zero slope if these parameters had no statistical variation and were independent of the sample cell length. These graphs can be considered as diagnostic diagrams since they can be used to identify instrumental problems and deficiencies. The average values of α and β for each measurement sequence as well as their standard deviations σ can be calculated using a computer fitting program. The values of ϵ' and ϵ'' for each measurement sequence are then calculated from the average values of α and β using eqs 5a and 5b. A data set at each temperature consists of the α, β, ϵ', and ϵ'' values obtained for a number of the measurement sequences outlined above. Average values of α, β, ϵ', and ϵ'' with their 1σ standard deviations summarize each data set. The relaxation time was calculated using the Cole–Cole equations (*13*) and method outlined previously (*11, 12*) as were the parameters characterizing the relaxation process.

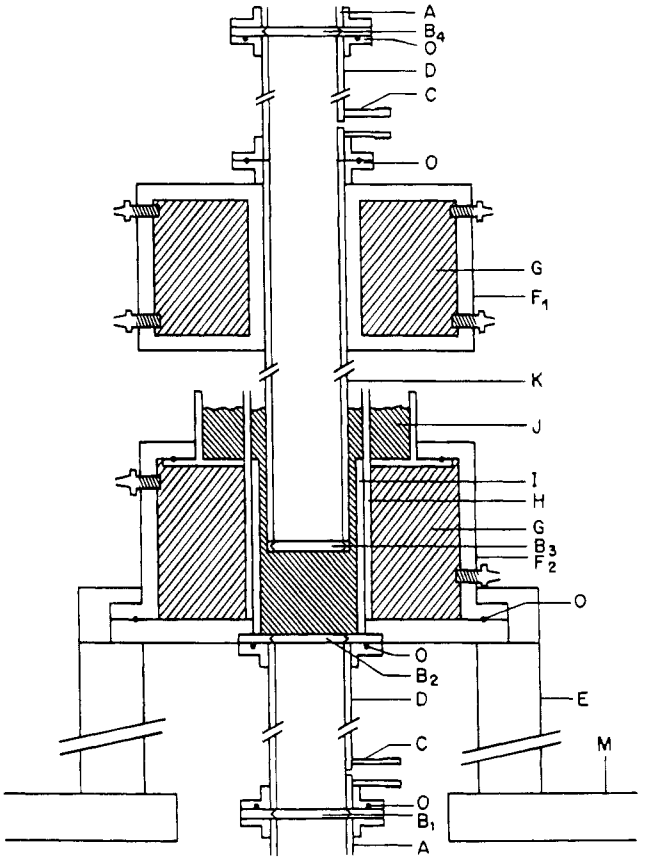

Figure 2. Schematic diagram for a 8.2–12.4 GHz variable-length transmission sample cell: (A) input waveguide, (B_1, B_2, B_4) waveguide windows (MDL-90WF56), (B_3) solderable waveguide window (MDL-90WD86), (C) evacuation port, (D) thin-wall stainless steel waveguide, (E) Tufnol thermal insulating system support, (F_1, F_2) upper and lower thermalizing jackets, (G) thermalizing fluid, (H) temperature measurement tube, (I) transmission sample cell outer waveguide (WR102), (J) sample fluid, (K) transmission sample cell inner waveguide (WR90), (M) main system support, (O) O-ring.

Description of the Instrumentation System

(1) Variable-Length Transmission Cell. Figure 2 is a schematic diagram for a variable-length transmission sample cell designed to operate in the 8.2–12.4 GHz waveguide band. It consists of four major components: (a) the microwave sample cell components, (b) the sample heating/cooling mechanism, (c) the thermal insulation of the sample cell, and (d) the sample cell incremental length mechanism.

(a) The sample cell consists of two waveguide sections. The lower fixed waveguide section consists of a length of gold-plated copper WR102 waveguide (I) with internal dimensions of 12.95 mm × 25.90 mm (0.510 in. × 1.020 in.) which was sealed with a commercial Kovar glass pressure window (B_2) and a 0.124 mm (0.005 in.) thick Teflon film gasket to prevent oxidation of the Kovar. The upper moveable waveguide section was a length of gold-plated copper WR90 waveguide (K) with external dimensions of 12.70 mm × 25.40 mm (0.500 in. × 1.000 in.) with

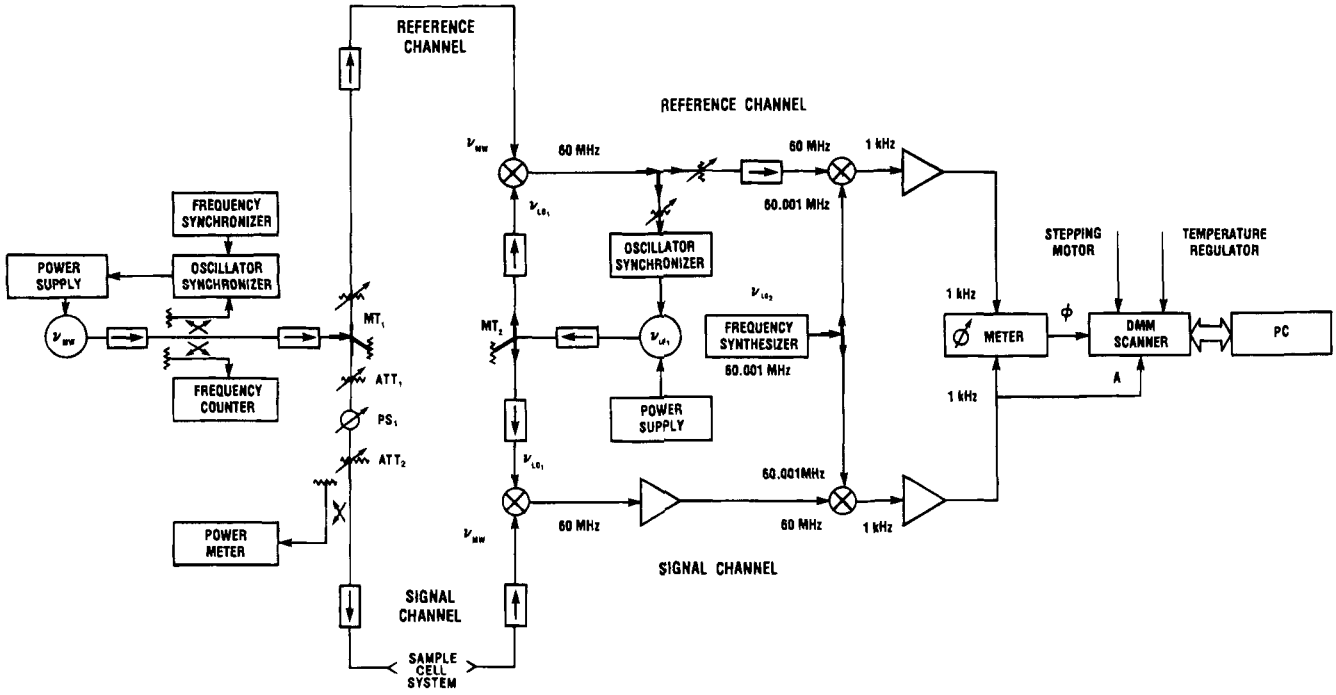

Figure 3. Schematic diagram for the dual-channel, double superheterodyne signal processing system.

another commercial Kovar glass pressure window (B_3) soldered to the lower end. The sample liquids under test were poured into the lower waveguide into which the upper moveable waveguide was inserted. Care was taken to ensure that no air bubbles were trapped on the bottom of window B_3. The microwave signal power entered the upper moveable waveguide, transmitted through the sample cell liquid, and exited through the lower fixed waveguide window (*8*, *10*, *12*).

(b) The sample cell liquid heating/cooling mechanism consists of two thermalizing jackets (F_1, F_2) attached to the upper moveable and lower fixed waveguide sections and a heating/cooling sample bath circulator and temperature controller (Haake F4-C). The temperature of the sample cell liquid under study can be varied from approximately 1 to 90 °C. The sample temperature can be set ±0.01 °C and regulated to better than ±0.003 °C using this temperature control system. However, ±2 °C fluctuations in the laboratory temperature are estimated to degrade this performance to about ±0.02 °C (*10*–*12*).

(c) The thermal insulation of the sample cell was introduced to minimize thermal gradients in the body of the sample cell. Two isolation sections consisting of 10 cm lengths of thin-wall (0.50 mm) stainless steel waveguide (D) sealed with waveguide windows (B_1, B_2 and B_3, B_4) and evacuated to prevent condensation of water vapor on the outer faces of the sample cell waveguide windows B_2 and B_3 were introduced to provide additional thermal isolation between the upper and lower waveguide sample cell sections and the remainder of the waveguide system.

(d) The sample cell length was incremented using a laboratory-designed 40 turn/in. precision micrometer driven by a computer-controlled stepping motor via a 23.6:1 geared reducer. The incremental error caused by the 200 step/turn stepping motor was eliminated by using one turn for each incremental step. The sample cell was incorporated into a special stand featuring two vertical 38.10 mm (1.5 in) diameter hollow ground rods. The lower fixed waveguide section of the sample cell was thermally isolated but attached to the lower portion of this stand. The upper moveable waveguide section of the sample cell was aligned inside the lower waveguide section and thermally isolated but attached to the lower surface of a counterbalanced plate, which could slide smoothly on the two vertical rods using linear ball bearing races. It was driven via a rotary-to-linear transducer consisting of a precision ball bearing by the geared reducer stepping motor and precision micrometer assembly. A fixed plate on which the precision micrometer and stepping motor were attached was locked at the top of the two vertical rods. The counterbalancing pulleys were attached to the top plate of the stand. See Photograph 2 of ref 10.

(2) Instrumentation System. A schematic diagram for the dual-channel, double superheterodyne signal processing system is given in Figure 3. The microwave signal power was obtained from a reflex klystron oscillator whose signal frequency was locked to a harmonic of the crystal oscillator frequency synthesizer (PTS-160) and divided into the reference channel and the signal channel. The signal channel included two precision rotary vane attenuators (ATT_1, ATT_2) (HP-X382A), a precision rotary vane phase shifter (PS_1) (HP-X885A), a flexible low loss microwave cable, and both ports between which the variable-length transmission sample cell would be inserted. The microwave power in the reference and signal channels were converted to a frequency of approximately 1 kHz via two frequency conversions. The 1 kHz amplitude and phase were measured using an 18 bit scanning DVM (Keithley 199 System) and a low-frequency precision digital phasemeter (Clarke Hess Model 6000), respectively. The amplitude and phase data as well as the sample cell temperature and the sample length were sent to a microcomputer via an IEEE-488 interface bus.

General Error Analysis Considerations

The primary error sources are in the measurement of the signal amplitude and phase, the mechanical and thermal stability of the sample cell, and the excitation of higher-order waveguide modes. Signal amplitude and phase measurement errors arise from mismatch errors at the input and output to the sample cell, signals at the output of the sample cell which are caused by leakage and microwave radiation signals, sample increment length errors, and frequency instability noise, while errors arising from the nonlinear response of the microwave and radio

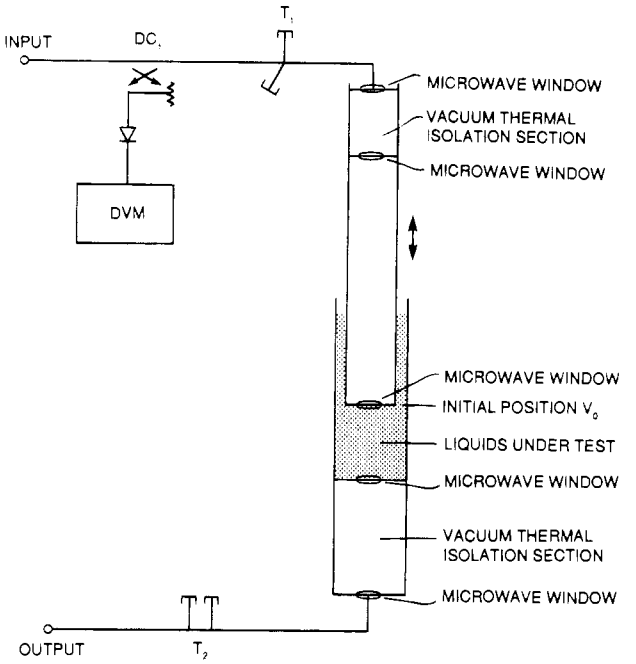

Figure 4. Schematic diagram for the sample cell microwave matching system.

frequency (rf) mixers can be neglected because they were operated in their linear regions.

It is difficult to carry out a complete error analysis for measurements of the complex permittivity of water from approximately 1 to 90 °C. The objective is to identify and minimize as many of the instrumentation system errors and then attempt to determine the most important main residual errors experimentally and to estimate the ultimate error limits for $\epsilon'(t)$ and $\epsilon''(t)$. Recent improvements to this instrumentation system are described below.

The mismatch error in the signal amplitude and phase measurement is caused by multiple reflections between the input and output ports of the sample cell and the insertion ports for the instrumentation system. An isolator with a very low VSWR (<1.05) and a double stub tuner were inserted between the instrumentation system ports and the upper and lower sample cell components as shown in Figure 4. A change in the temperature of the sample liquid changes the input and output impedances of the sample cell. These changes arise because the sample cell behaves like an impedance transformer section. However, changing the sample cell length at each temperature has a much smaller effect on the impedance of this section than changing the temperature. Consequently, the input tuner T_1 must be adjusted to minimize the VSWR of the input port when the sample liquid temperature is changed. For convenience, a multihole directional coupler and detector was connected in front of the tuner T_1, as shown in Figure 4, to monitor the reflected wave from the sample cell using a $3^1/_2$ digit DVM. This also enabled the sample cell and the liquid level to be monitored. Large variations of the dc signal are indicative of misaligned sample cell waveguide sections or the existence of air bubbles on the waveguide window. The input impedance at the sample cell output port was found to be essentially independent of variations in the temperature and length of the sample cell liquid. Consequently, tuner T_2 did not require readjustment when measurements were made at different temperatures.

The incremental differential diagrams for α and β obtained for a measurement sequence can be used as a diagnostic tool to identify instrumentation system deficiencies. Consequently, they can be used as intuitive judgement criteria to adjust and improve the instrumentation system. Parts a and b of Figure 5 give the incremental differential diagrams for α and β, respectively, when the sample length increment is zero, i.e., the sample length remains unchanged but 500 signal amplitude and phase data pairs are acquired at a 3 s sampling rate. The sample cell length was located at increment step numbers 0 and 300 for the measurements given in parts a and b of Figure 5, respectively. These diagrams show the random errors of the instrumentation system which are caused by the frequency instability and the noise of the signal processing instrumentation system. Parts a and b of Figure 6 give the incremental differential diagrams when $\alpha = 347.6$ Np·m^{-1} and $\beta = 1598.3$ rad·m^{-1}, respectively. An error analysis of eqs 4a and 4b yields

$$\frac{\Delta\alpha}{\alpha} = \frac{1}{\ln A}\frac{dA}{A} - \frac{dz}{z} \tag{6a}$$

$$\frac{\Delta\beta}{\beta} = \frac{d\phi}{\phi} - \frac{dz}{z} \tag{6b}$$

where $A = A_n/A_{n+1}$ and $\phi = \phi_n - \phi_{n+1}$. It can be seen from eqs 6a and 6b that the errors of α and β in Figure 6 arise from dA/A, $d\phi/\phi$, and dz/z, i.e., the fractional errors in the signal amplitude and phase and the cell incremental length. Comparing the diagrams in Figure 6 with those in Figure 5 shows that the former two errors are greater than the latter. This has been verified experimentally by checking the reliability and drive error of the mechanism which increments the length of the sample cell. Figure 7

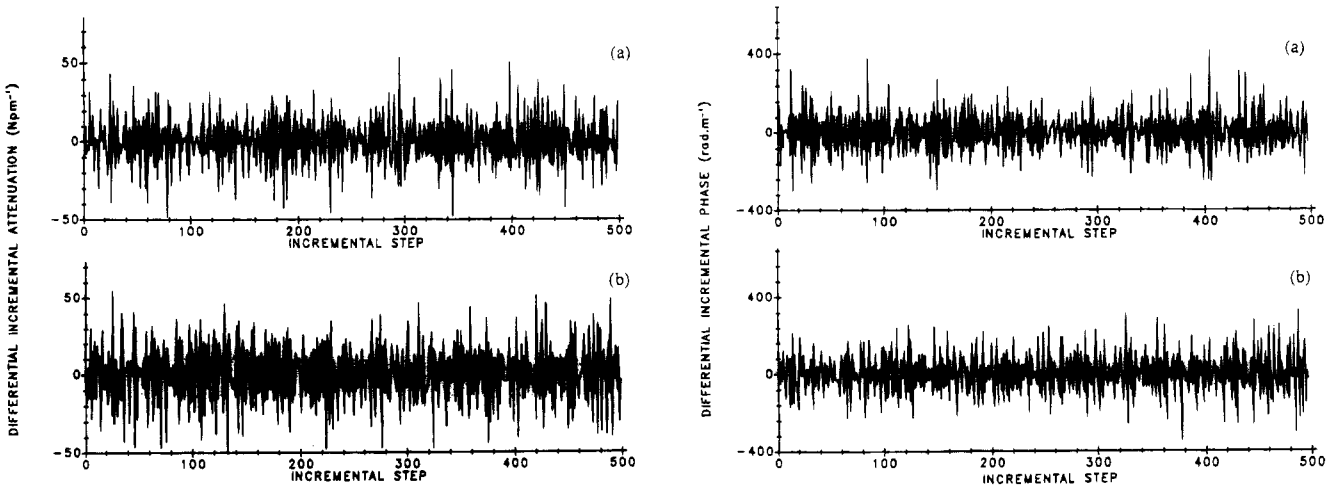

Figure 5. Incremental differential diagrams for α and β when the sample cell length is fixed at increment step (a) 0 and (b) 300.

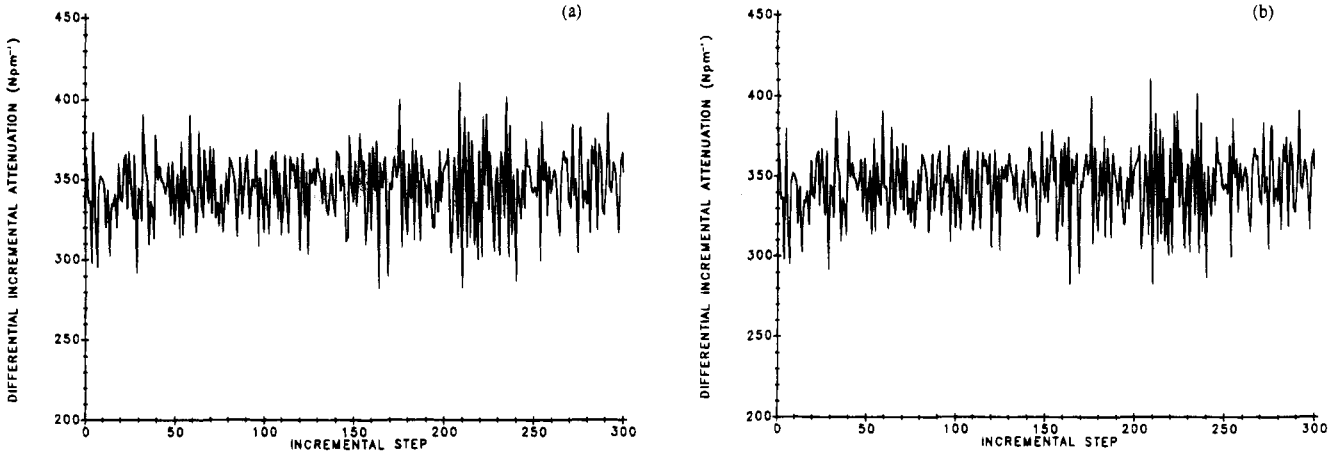

Figure 6. Incremental differential diagrams for (a) α = 347.6 Np m^{-1} and (b) β = 1598.3 rad m^{-1}.

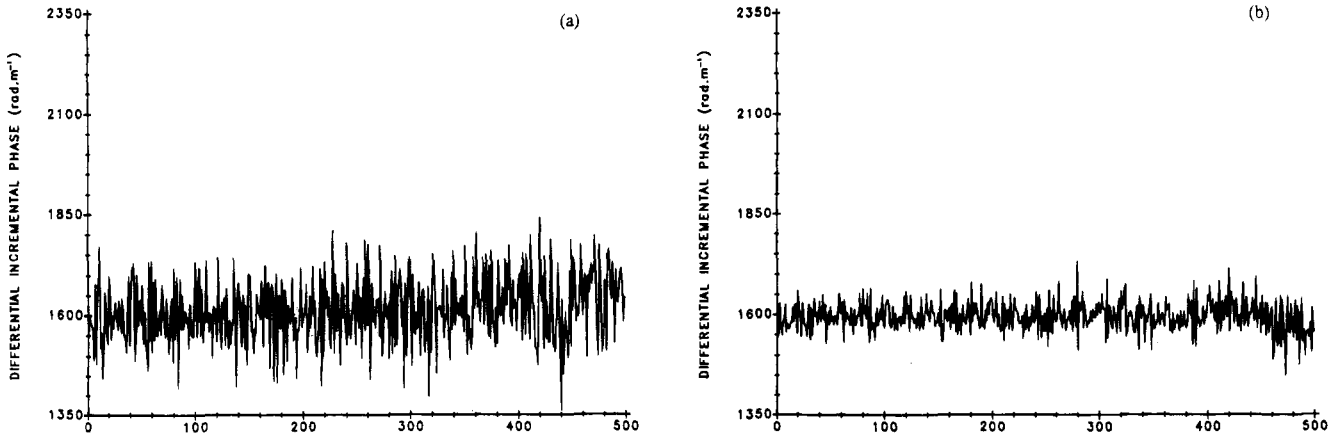

Figure 7. Incremental differential diagram for β using (a) a phase-sensitive amplifier (Ithaco Dynatrac 3 with phase option) and (b) a digital phase meter (Clarke-Hess Model 6000).

shows the improvement in the incremental differential diagram for β when a digital phase meter (Clarke-Hess Model 6000) replaced the 1 kHz synchronous demodulator (lock-in amplifier) as the instrument used to measure the signal phase at 1 kHz. This digital phase meter has a resolution of 0.01° and a repeatability of ±0.01° and was calibrated by its manufacturer using a NITS secondary standard. It was not used to make absolute phase measurements because it is the difference between measurements made at successive increments that is required to calculate β. Consequently, the resolution and short-term stability are the most important performance specifications. It is evident by comparison with Figures 5b and 6b that a statistical improvement of more than a factor of 3 has been achieved.

Minimization of the Leakage and Determination of the Residual Errors

Another improvement that has been accomplished using the incremental differential diagram is the minimization of the microwave leakage and radiation effects. Ripples in these diagrams are an indicator of the existence of undesired leakage signals in the output of the sample cell (*9*, *11*, *12*), as Figure 8a shows. These ripples appear when a large number of increment steps are used at the low signal-to-noise ratio end of the diagram. An analysis of these ripples is as follows.

If an undesired leakage signal exists at the output of the sample cell which is denoted by $v_e = A_e e^{j\phi_e}$, then the measured values of α and β at increment step number n (denoted by α_n and β_n, respectively) are given by

$$e^{(\alpha_n+j\beta_n)z} = \frac{v_n + v_e}{v_{n+1} + v_e} = \frac{A_o e^{j\phi_o} e^{-(\alpha+j\beta)nz} + A_e e^{j\phi_e}}{A_o e^{j\phi_o} e^{-(\alpha+j\beta)(n+1)z} + A_e e^{j\phi_e}} \quad (7)$$

where

$$\phi_n = \beta nz + \phi_e - \phi_o \quad (8a)$$

$$\phi_{n+1} = \beta(n+1)z + \phi_e - \phi_o \quad (8b)$$

and

$$E = A_e/A_o \quad (8c)$$

A_e and ϕ_e are the amplitude and phase of the undesired leakage signal and A_o and ϕ_o are the amplitude and phase of the signal at the initial sample cell length. Substituting eqs 8a–8c into eq 7 yields

$$e^{(\alpha_n+j\beta_n)z} = \frac{e^{-\alpha nz} e^{-j\phi_n} + E}{e^{-\alpha(n+1)z} e^{-j\phi_{n+1}} + E} \quad (9)$$

Solving eq 9 for α_n and β_n yields

$$\alpha_n = \frac{1}{2z} \times \ln\left[\frac{(e^{-\alpha nz}\cos\phi_n + E)^2 + (e^{-\alpha nz}\sin\phi_n)^2}{(e^{-\alpha(n+1)z}\cos\phi_{n+1} + E)^2 + (e^{-\alpha(n+1)z}\sin\phi_{n+1})^2}\right] \quad (10)$$

and

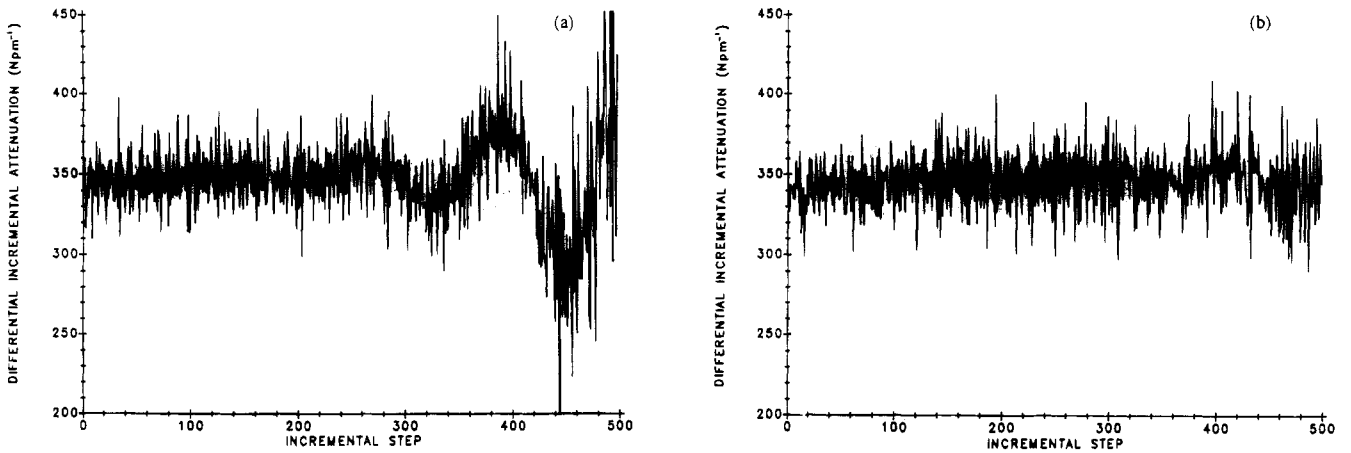

Figure 8. Incremental differential diagrams for α and β when (a) the leakage signal causes ripples and (b) after reduction of the leakage signal.

$$\beta_n = \frac{1}{z}\left\{\tan^{-1}\left[\frac{e^{-\alpha(n+1)z}\sin\phi_{n+1}}{e^{-\alpha(n+1)z}\cos\phi_{n+1}+E}\right] - \tan^{-1}\left[\frac{e^{-\alpha nz}\sin\phi_n}{e^{-\alpha nz}\cos\phi_n+E}\right]\right\} \quad (11)$$

Equations 10 and 11 include the influence of the undesired leakage signal. If the ratio $E = 0$, then $\alpha_n = \alpha$ and $\beta_n = \beta$; i.e., the values of α_n and β_n are independent of the increment step number n and the measurements lead to incremental differential diagrams with no ripples. However, if $E \neq 0$, then the values of α_n and β_n will be functions of the increment step number n and the incremental differential diagrams will have ripples. Computer simulations using eqs 10 and 11 yield curves whose ripples are very similar to those of the incremental differential diagrams for α and β in Figure 8. These computer simulations also show that the amplitude of the ripples is a function of ϕ_0 and that the amplitude of the ripples can be minimized by the correct choice of ϕ_0. However, it is preferable to minimize the ripples by minimizing the undesired signal caused by leakage and radiation. This was a subtle task, but the main sources of the leakage and radiation were identified using a spectrum analyzer (Tektronix 7838 with 7L18 plug-in) and microwave horn as a probe. These sources were found to be the reflex klystron oscillator and the precision rotary vane attenuators (ATT_1, ATT_2) and phase shifter (PS_1). Shielding these sources resulted in improved incremental differential diagrams for α and β as Figure 8b shows.

The initial phase ϕ_0 is a function of the initial sample cell length which is selected before the measurement process starts and is temperature dependent. ϕ_0 can also be varied by adjusting the phase shifter PS_1 in the signal channel (see Figure 3). The values of α and β should be independent of ϕ_0. Consequently, the presence of undesired leakage and mismatch signals can be determined from the values of α and β obtained using this phase shifter to vary ϕ_0. The deviation of α and β from ideal behavior enables the measurement accuracy to be estimated. Table 1 gives the values of α and β as a function of the initial phase ϕ_0 for the double-distilled, deionized light water at (a) 25.13 °C and (b) 72.47 °C. The maximum fractional errors of α and β, $\Delta\alpha/\alpha$ and $\Delta\beta/\beta$, are ±0.06% and ±0.03% at 25.13 °C and ±0.09% and ±0.03% at 72.47 °C, respectively. The uncertainty in the complex permittivity introduced by these measurement errors in α and β can be estimated from

$$\frac{\Delta\epsilon'}{\epsilon'} = \frac{1}{\epsilon'}\left[\left(\frac{\partial\epsilon'}{\partial\beta}\Delta\beta\right)^2 + \left(\frac{\partial\epsilon'}{\partial\alpha}\Delta\alpha\right)^2\right]^{1/2} \quad (12a)$$

Table 1. Effect of Varying the Precision Rotary Vane Phase Shifter in the Signal Channel on the Measured Values of α and β and the Calculated Values of ε′ and ε″ at 25.13 and 72.47 °C

φ/deg	α/(Np·m⁻¹)	β/(rad·m⁻¹)	ε′	ε″
		(a) 25.13 °C		
26	344.532(32)	1598.608(106)	63.772	28.655
56	344.738(47)	1599.388(99)	63.833	28.689
86	344.991(41)	1600.329(78)	63.907	28.724
116	345.054(44)	1599.885(96)	63.869	28.721
146	345.109(37)	1599.943(86)	63.873	28.727
176	344.883(40)	1599.153(97)	63.812	28.694
206	344.574(37)	1599.347(96)	63.833	28.671
236	344.704(33)	1599.294(1050	63.826	28.981
266	344.611(29)	1599.509(91)	63.846	28.677
296	344.670(29)	1599.445(87)	63.840	28.681
326	344.505(33)	1599.068(97)	63.811	28.661
356	344.692(30)	1598.955(83)	63.798	28.674
	344.759(197)	1599.410(449)	63.835(35)	28.688(23)
		(b) 72.47 °C		
0	131.078(66)	1529.937(102)	60.825	10.433
23	131.218(71)	1529.435(98)	60.784	10.441
53	131.114(71)	1529.266(94)	60.771	10.432
83	131.173(67)	1529.691(97)	60.804	10.439
113	131.212(71)	1530.031(99)	60.831	10.445
143	131.223(74)	1530.086(99)	60.836	10.446
173	131.321(70)	1528.960(93)	60.745	10.446
203	131.155(75)	1530.091(96)	60.836	10.441
233	131.081(77)	1530.060(101)	60.834	10.434
263	131.076(82)	1530.123(93)	60.839	10.434
293	130.797(69)	1528.967(89)	60.749	10.404
323	131.138(66)	1530.086(91)	60.836	10.439
353	130.823(66)	1528.923(97)	60.746	10.406
	131.108(144)	1529.666(469)	60.803(37)	10.434(13)

$$\frac{\Delta\epsilon''}{\epsilon''} = \frac{1}{\epsilon''}\left[\left(\frac{\partial\epsilon''}{\partial\beta}\Delta\beta\right)^2 + \left(\frac{\partial\epsilon''}{\partial\alpha}\Delta\alpha\right)^2\right]^{1/2} \quad (12b)$$

Combining eqs 5a, 5b, 12a, and 12b yields

$$\frac{\Delta\epsilon'}{\epsilon'} = \frac{2}{\epsilon'}\left(\frac{\lambda}{2\pi}\right)^2\left[\left(\beta^2\frac{\Delta\beta}{\beta}\right)^2 + \left(\alpha^2\frac{\Delta\alpha}{\alpha}\right)^2\right]^{1/2} \quad (13a)$$

$$\frac{\Delta\epsilon''}{\epsilon''} = \left[\left(\frac{\Delta\beta}{\beta}\right)^2 + \left(\frac{\Delta\alpha}{\alpha}\right)^2\right]^{1/2} \quad (13b)$$

At 9.355 GHz, eq 13a becomes

$$\frac{\Delta\epsilon'}{\epsilon'} = \frac{52.026}{\epsilon'}\left[\left(\beta^2\frac{\Delta\beta}{\beta}\right)^2 + \left(\alpha^2\frac{\Delta\alpha}{\alpha}\right)^2\right]^{1/2} \quad (13c)$$

According to eqs 13b and 13c, the uncertainties of the complex permittivity introduced by the measurement errors of α and β are $\Delta\epsilon'/\epsilon' = \pm 0.05\%$ and $\Delta\epsilon''/\epsilon'' = \pm 0.08\%$ for 25.13 °C and $\Delta\epsilon'/\epsilon' = \pm 0.06\%$ and $\Delta\epsilon''/\epsilon'' = \pm 0.1\%$ for 72.47 °C.

Experimental Results and Discussion

The measured values of the attenuation coefficient $\alpha(t)$, the phase shift coefficient $\beta(t)$, the permittivity $\epsilon'(t)$, and the dielectric loss $\epsilon''(t)$ and their standard deviations for double-distilled, deionized light water and heavy water at 9.355 GHz in the temperature interval from approximately 1 to 90 °C are listed in Table 2. Parts a and b of Figure 9 are graphs of the permittivity $\epsilon'(t)$ and dielectric loss $\epsilon''(t)$ as a function of the temperature, respectively, for both light and heavy water. The permittivity of heavy water is less than that of light water at all temperatures whereas the dielectric loss is greater for heavy than for light water except below about 5 °C. The data in Table 2 were fitted to empirical quintic polynomials in the temperature t (°C) using the method of least squares given by Press et al. (*15*):

(a) light water

$$\epsilon'(t) = 44.628(3) + (13.929(8) \times 10^{-1})t - (3.222(6) \times 10^{-2})t^2 + (3.165(17) \times 10^{-4})t^3 - (1.503(21) \times 10^{-6})t^4 + (2.67(9) \times 10^{-9})t^5 \quad (14a)$$

$$\epsilon'(t) = 40.573(3) - (1.475(6) \times 10^{-1})t - (2.477(4) \times 10^{-2})t^2 + (6.092(12) \times 10^{-4})t^3 - (6.000(15) \times 10^{-6})t^4 + (2.213(7) \times 10^{-8})t^5 \quad (14b)$$

$$\alpha(t) = 550.389(35) - 7.699(6)t - (1.016(4) \times 10^{-1})t^2 + (4.531(12) \times 10^{-3})t^3 - (5.522(15) \times 10^{-5})t^4 + (2.352(7) \times 10^{-7})t^5 \quad (14c)$$

$$\beta(t) = 1416.305(46) + 14.870(9)t - (4.078(7) \times 10^{-1})t^2 + (4.884(19) \times 10^{-3})t^3 - (3.026(24) \times 10^{-5})t^4 + (7.64(11) \times 10^{-8})t^5 \quad (14d)$$

(b) heavy water

$$\epsilon'(t) = 31.452(17) + (16.630(28) \times 10^{-1})t - (2.796(17) \times 10^{-2})t^2 + (1.141(45) \times 10^{-4})t^3 + (0.920(54) \times 10^{-8})t^4 - (7.16(23) \times 10^{-9})t^5 \quad (15a)$$

$$\epsilon''(t) = 37.610(9) + (4.952(16) \times 10^{-1})t - (4.749(10) \times 10^{-2})t^2 + (9.659(26) \times 10^{-4})t^3 - (8.609(30) \times 10^{-6})t^4 + (2.913(13) \times 10^{-8})t^5 \quad (15b)$$

$$\alpha(t) = 587.35(10) - 4.537(18)t - (2.247(11) \times 10^{-1})t^2 + (5.759(29) \times 10^{-3})t^3 - (5.309(34) \times 10^{-5})t^4 + (1.764(14) \times 10^{-7})t^5 \quad (15c)$$

$$\beta(t) = 1244.84(22) + 22.088(36)t - (5.592(21) \times 10^{-1})t^2 + (6.841(55) \times 10^{-3})t^3 - (4.516(64) \times 10^{-5})t^4 + (1.254(27) \times 10^{-7})t^5 \quad (15d)$$

It is noted that the 1σ errors for these coefficients are about a factor of 3 greater for those polynomial expressions associated with heavy rather than light water. No explanation can be offered except that the former measurements were made after the latter. The values of α, β, ϵ', and ϵ'' given in Table 2 are the average of the values obtained from data sets consisting of three measurement sequences at each temperature. The standard deviations of α, β, ϵ', and ϵ'' were calculated using $\sigma = [\sum(x - \bar{x})^2/(n-1)]^{1/2}$ where $n = 3$. Each measurement sequence was started at the same initial sample cell length. The distance between this initial length and the window in the lower waveguide was 8.255 mm (0.325 in.) to minimize the effect of reflections from this window. The length of each sample cell increment was $z = 0.6350/23.6 = 0.026\,91$ mm. It was found that the addition of the 23.6:1 geared coaxial reducer decreased the incremental length error but increased the time required to make a measurement sequence from approximately 1.5 to approximately 3 s per increment. After each sample cell length increment, the amplitude and phase of the microwave signal transmitted through the liquid under investigation were measured and recorded. It was found to be necessary to select the total number of measurement intervals so that the total incremental sample cell length was approximately one or one and a half wavelengths to eliminate the first-order error due to the presence of residual ripple. The calculated 9.355 GHz guide wavelength in light water at 25 °C is 5.11 mm. Therefore, the incremental step number n should be $5.11/z \simeq 190$ or $(5.11/z) \times 1.5 \simeq 285$. This length was verified experimentally by plotting the 1σ error as a function of the total step number. It was found that a broad minimum existed centered on 190 and 285. However, each measurement sequence consisted of 320 increments from the initial sample cell length because the sample cell temperature was inferred to change by a very small (0.01 °C) but detectable amount when the length was rapidly returned to its initial length. The first 40 incremental steps were deleted to ensure that the cell temperature returned to its equilibrium value and to eliminate any backlash in the micrometer thread and the geared reducer that occurs due to reversing the direction of rotation. The standard deviations of $\alpha(t)$ and $\beta(t)$ obtained from single-measurement sequences depend on the number of increment steps used. If the same number of increment steps is used, then their values are correlated with the quality of the incremental differential diagrams for these sequences.

The data in Table 2 were obtained using a sample cell with a 1.0 mm wide longitudinal slit in the middle of each broad face of the lower fixed waveguide. These slits were introduced to eliminate any undesired higher-order modes which may be excited. Comparison of these results with those obtained using another sample cell without these longitudinal slits did not reveal any detectable difference.

The standard deviations σ of the average values of $\alpha(t)$ and $\beta(t)$ for each measurement sequence are typically 0.004–0.008% for $\beta(t)$ in the temperature interval from approximately 1 to 90 °C and 0.014–0.018% for $\alpha(t)$ up to 60 °C. The σ values for α degraded at temperatures above 60 °C and became approximately 0.07% above 80 °C in confirmation of the conclusion of Barajas and Buckmaster (*11*). The reason for this degradation at high temperatures for light water may be due to thermal deformation of the 0.125 mm thick Teflon gasket covering the lower, fixed waveguide section of the sample cell or the presence of water vapor bubbles (*11*). Further improvements to the sample cell are in progress to eliminate these and other problems.

The 1σ standard deviations of $\alpha(t)$, $\beta(t)$, $\epsilon'(t)$, and $\epsilon''(t)$ given in Table 2 represent the repeatability of multiple measurements and depend primarily on the following factors: the temperature stability of the liquid being studied, the reproducibility of the sample cell length increment of the sample cell, and the frequency stability of the phase lock loops in the instrumentation system. It can be concluded that the typical 1σ standard deviations for $\epsilon'(t)$ and $\epsilon''(t)$ are $\simeq$0.02% and their accuracies are about 0.1%.

Table 2. Attenuation Coefficient α, Phase Coefficient β, Permittivity ε′, and Dielectric Loss ε″ and Their Standard Deviations for Double-Distilled, Deionized Water and Heavy Water at 9.355 GHz

t/°C	α/(Np·m^{-1})	β/(rad·m^{-1})	ε′	ε″	t/°C	α/(Np·m^{-1})	β/(rad·m^{-1})	ε′	ε″
				(a) Double-Distilled, Deionized Water at 0–90 °C					
0.25	547.102(40)	1419.273(48)	44.995(3)	40.398(5)	47.49	216.911(98)	1591.258(108)	65.027(10)	17.957(8)
2.59	529.169(55)	1452.468(115)	47.977(10)	39.987(3)	49.98	206.799(7)	1586.859(120)	64.774(10)	17.073(2)
5.17	508.931(44)	1482.307(104)	50.802(8)	39.248(6)	52.47	196.121(45)	1583.682(94)	64.624(8)	16.159(5)
7.43	489.380(60)	1506.687(196)	53.205(15)	38.361(8)	54.97	183.108(85)	1576.286(114)	64.145(9)	15.016(7)
10.07	467.007(37)	1529.784(105)	55.586(9)	37.169(1)	57.47	174.479(60)	1570.319(48)	63.736(5)	14.255(5)
12.45	446.481(8)	1547.381(123)	57.482(10)	35.944(2)	59.97	166.236(116)	1562.966(157)	63.210(12)	13.518(11)
15.07	424.354(81)	1563.320(73)	59.273(6)	34.514(7)	62.47	158.889(14)	1557.310(85)	62.813(7)	12.873(1)
17.47	404.216(31)	1575.564(22)	60.707(2)	33.134(2)	64.97	151.373(23)	1549.662(172)	62.256(13)	12.204(3)
19.86	384.858(94)	1585.635(153)	61.933(13)	31.749(8)	67.47	144.757(76)	1542.831(55)	61.757(4)	11.619(6)
22.46	364.628(18)	1593.439(187)	62.973(15)	30.228(5)	69.97	138.123(18)	1535.607(83)	61.227(7)	11.035(2)
24.99	345.529(14)	1598.877(134)	63.777(12)	28.742(2)	72.47	130.971(66)	1529.353(115)	60.779(9)	10.421(6)
27.47	326.595(66)	1602.584(87)	64.417(7)	27.230(6)	74.97	126.605(126)	1521.096(53)	60.153(3)	10.019(10)
30.02	310.447(34)	1604.201(18)	64.819(1)	25.910(3)	77.47	119.873(54)	1515.081(59)	59.721(5)	9.449(4)
32.47	294.559(23)	1605.352(191)	65.165(16)	24.601(3)	79.97	115.509(37)	1507.298(173)	59.136(14)	9.058(2)
34.79	280.900(61)	1604.696(75)	65.315(8)	23.451(4)	82.47	113.285(79)	1500.860(65)	58.645(5)	8.846(6)
37.47	265.730(65)	1603.207(189)	65.406(15)	22.164(8)	84.97	107.246(84)	1492.351(18)	58.017(2)	8.327(7)
39.98	252.619(59)	1601.356(44)	65.429(3)	21.046(5)	87.47	103.022(55)	1485.969(23)	57.546(2)	7.965(5)
42.47	240.034(105)	1597.925(46)	65.305(5)	19.955(8)	90.00	98.368(82)	1477.156(47)	56.891(4)	7.560(7)
44.97	228.487(93)	1594.380(184)	65.151(14)	18.953(10)					
				(b) Heavy Water at 4–90 °C					
4.00	564.101(88)	1324.925(149)	37.769(9)	38.884(10)	47.49	255.274(61)	1565.921(100)	62.474(8)	20.797(6)
5.17	557.663(69)	1344.188(205)	39.294(16)	38.999(5)	49.98	242.860(60)	1563.714(179)	62.456(60)	19.758(3)
7.43	543.506(53)	1379.908(258)	42.231(20)	39.019(6)	52.47	231.614(88)	1558.816(78)	62.197(6)	18.784(8)
10.07	524.612(32)	1417.982(64)	45.527(5)	38.702(2)	54.97	220.605(141)	1555.378(63)	62.048(6)	17.851(11)
12.45	506.957(92)	1444.848(121)	48.002(7)	38.108(10)	57.47	210.293(63)	1550.633(128)	61.780(10)	16.965(6)
15.07	485.716(76)	1471.728(26)	50.589(1)	37.191(7)	59.97	200.578(64)	1546.335(192)	61.537(13)	16.136(6)
17.47	465.590(35)	1492.023(63)	52.652(6)	36.141(2)	62.47	191.277(104)	1540.800(136)	61.188(12)	15.333(8)
19.86	446.496(30)	1509.753(88)	54.490(7)	35.071(4)	64.97	181.693(53)	1535.891(168)	60.888(13)	14.518(6)
22.46	424.337(96)	1525.753(152)	56.255(11)	33.684(10)	67.47	173.231(24)	1530.225(21)	60.514(2)	13.791(2)
24.99	404.202(117)	1538.746(98)	57.725(6)	32.358(11)	69.97	165.098(226)	1523.508(90)	60.052(8)	13.086(18)
27.47	383.744(127)	1548.534(117)	58.930(11)	30.916(10)	72.47	157.578(111)	1517.745(257)	59.659(20)	12.443(11)
30.02	364.538(142)	1555.744(74)	59.886(4)	29.506(13)	74.97	150.256(164)	1510.102(169)	59.116(13)	11.805(14)
32.47	346.555(53)	1561.427(294)	60.680(23)	28.152(9)	77.47	143.596(228)	1503.724(205)	58.667(15)	11.234(19)
34.79	330.181(38)	1565.031(80)	61.261(7)	26.884(2)	79.97	138.844(43)	1496.938(59)	58.172(4)	10.813(4)
37.47	312.808(196)	1568.540(179)	61.838(17)	25.527(14)	82.47	132.733(77)	1489.813(161)	57.661(13)	10.288(5)
39.98	296.930(112)	1569.074(186)	62.133(14)	24.239(12)	84.97	125.791(137)	1482.322(31)	57.129(2)	9.701(11)
42.47	282.331(108)	1569.265(90)	62.369(6)	23.050(10)	87.47	120.649(97)	1475.187(186)	56.613(14)	9.260(8)
44.97	268.752(73)	1568.616(250)	62.510(19)	21.933(9)	90.00	115.644(37)	1468.095(109)	56.101(9)	8.833(3)

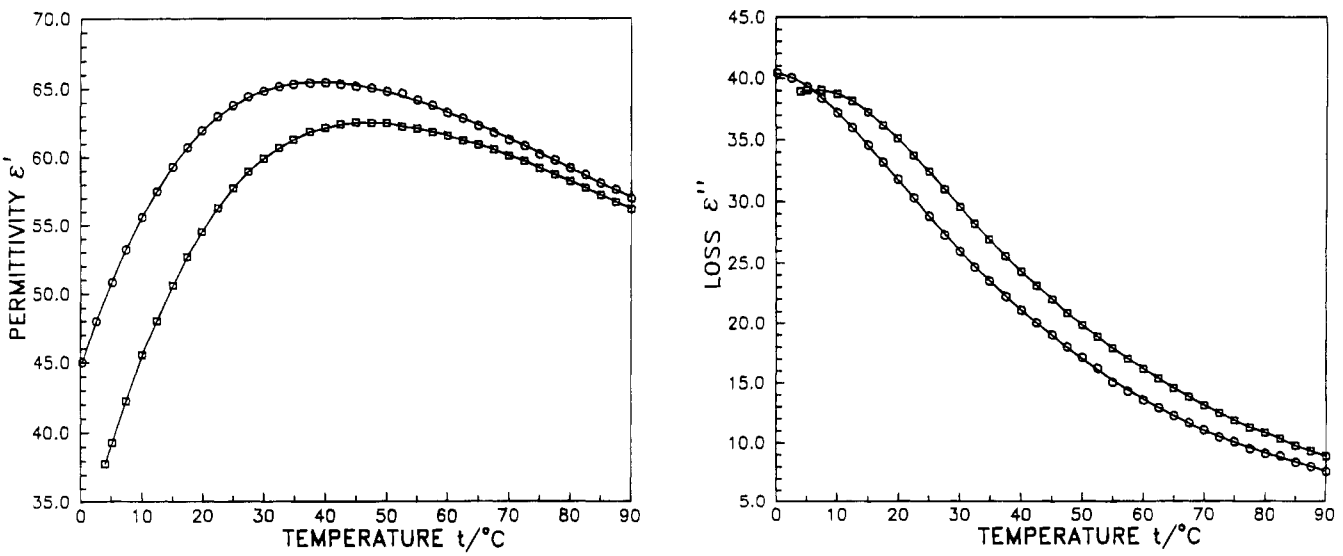

Figure 9. Graphs of (a, left) the permittivity $\epsilon'(t)$ and (b, right) the dielectric loss $\epsilon''(t)$ as a function of the temperature at 9.355 GHz for light (○) and heavy (□) water.

Comparison of eqs 14a and 14b with those reported by Barajas and Buckmaster (*11*) for data obtained over the same temperature interval shows that the standard deviations of the coefficients have decreased by a factor of at least 2. This improvement has been achieved using data sets at each temperature consisting of three rather than seventeen measurement sequences. The acquisition time for each data set was decreased by only a factor of about 3 because the acquisition time for each measurement sequence increased by a factor of about 2. This confirms that both the precision and accuracy could have been improved by a factor of about 4 if 17 measurement sequences had been used.

The temperature dependence of the enthalpy (ΔH^*) and the entropy (ΔS^*) of activation for the relaxation process parameters were determined by assuming that these parameters were constant over approximately 8 °C temperature intervals. This assumption was necessary in order to calculate the values of these parameters from the values of the α and β parameters measured at a single

Table 3. Values for the Enthalpy of Activation ΔH^* and Their Standard Deviations for Double-Distilled, Deionized Water and Heavy Water at 9.355 GHz[a]

	$\alpha = 0.013$ and $\epsilon_\infty = 4.25$ [from Mason et al. (16)]		$\alpha = 0$ and ϵ_∞ (eq 4) [from Kaatze (17)]			$\alpha = 0.013$ and $\epsilon_\infty = 4.25$ [from Mason et al. (16)]		$\alpha = 0$ and ϵ_∞ (eq 4) [from Kaatze (17)]	
t/°C	$\Delta H^*_{\epsilon'}$/ (kJ·mol^{-1})	$\Delta H^*_{\epsilon''}$/ (kJ·mol^{-1})	$\Delta H^*_{\epsilon'}$/ (kJ·mol^{-1})	$\Delta H^*_{\epsilon''}$/ (kJ·mol^{-1})	t/°C	$\Delta H^*_{\epsilon'}$/ (kJ·mol^{-1})	$\Delta H^*_{\epsilon''}$/ (kJ·mol^{-1})	$\Delta H^*_{\epsilon'}$/ (kJ·mol^{-1})	$\Delta H^*_{\epsilon''}$/ (kJ·mol^{-1})
				(a) Double-Distilled, Deionized Water at 5–85 °C					
5.17	19.63(2)	11.26(3)	19.36(1)	10.79(3)	47.49	16.51(8)	14.19(5)	15.79(7)	14.14(5)
7.43	18.93(2)	14.28(3)	18.59(2)	13.57(3)	49.98	16.43(13)	16.14(6)	15.68(12)	16.05(6)
10.07	18.49(2)	16.31(4)	18.11(2)	15.70(4)	52.47	14.64(10)	17.16(4)	13.96(10)	17.07(4)
12.45	17.88(2)	16.65(1)	17.46(2)	16.14(1)	54.97	13.29(13)	17.29(4)	12.66(13)	17.20(4)
15.07	17.79(2)	16.66(1)	17.36(2)	16.15(1)	57.47	11.78(13)	15.21(3)	11.22(13)	15.22(3)
17.47	17.60(3)	16.62(2)	17.15(3)	16.18(2)	59.97	12.14(17)	13.75(4)	11.54(16)	13.81(4)
19.86	17.22(3)	16.54(2)	16.74(3)	16.19(2)	62.47	11.41(10)	13.80(5)	10.83(9)	13.87(5)
22.46	16.78(2)	16.61(2)	16.29(2)	16.25(2)	64.97	11.28(18)	13.85(3)	10.70(17)	13.95(3)
24.99	15.82(3)	16.36(2)	15.33(3)	16.07(2)	67.47	11.50(19)	13.96(3)	10.90(18)	14.06(3)
27.47	15.53(4)	16.17(2)	15.03(4)	15.90(2)	69.97	11.54(13)	13.67(6)	10.91(13)	13.79(6)
30.02	15.25(5)	15.95(2)	14.73(5)	15.70(2)	72.47	12.80(12)	14.28(6)	12.10(12)	14.43(6)
32.47	15.06(5)	15.24(3)	14.54(5)	15.04(3)	74.97	14.31(25)	13.42(3)	13.46(23)	13.61(3)
34.79	15.12(2)	15.06(3)	14.57(2)	14.89(3)	77.47	17.10(22)	11.30(8)	16.06(21)	11.55(8)
37.47	14.64(6)	14.75(3)	14.08(5)	14.60(3)	79.97	14.36(11)	10.11(11)	13.49(10)	10.42(11)
39.98	14.56(6)	14.62(4)	14.00(6)	14.49(4)	82.47	14.91(16)	10.31(8)	19.54(36)	10.63(8)
42.47	14.51(9)	14.46(5)	13.93(8)	14.36(5)	84.97	16.04(26)	11.10(7)	19.54(60)	11.42(7)
44.97	14.75(7)	14.19(3)	14.14(7)	14.12(3)					
				(b) Heavy Water at 7–85 °C					
7.43	21.68(2)	9.98(8)	21.50(2)	−11.95(7)	47.49	13.67(5)	15.20(5)	13.18(5)	15.06(5)
10.07	20.17(1)	4.25(9)	19.89(1)	−5.62(7)	49.98	13.22(8)	15.04(6)	12.73(8)	14.93(6)
12.45	19.80(2)	11.95(4)	19.50(1)	10.78(3)	52.47	13.20(8)	14.60(5)	12.70(8)	14.53(4)
15.07	19.52(1)	13.18(4)	19.20(1)	11.97(3)	54.97	13.37(13)	14.43(4)	12.85(12)	14.38(4)
17.47	18.98(2)	16.60(7)	18.61(2)	15.59(7)	57.47	13.63(11)	14.32(7)	13.08(10)	14.30(6)
19.86	18.63(1)	16.99(6)	18.23(1)	16.12(5)	59.97	13.38(12)	14.68(7)	12.84(12)	14.68(6)
12.46	18.33(2)	17.38(4)	17.90(2)	16.60(4)	62.47	13.96(9)	14.84(4)	13.36(8)	14.86(4)
24.99	17.59(2)	18.05(5)	17.14(2)	17.37(5)	64.97	13.49(15)	15.01(5)	12.90(15)	15.04(5)
27.47	17.16(3)	17.56(6)	16.70(3)	17.05(6)	67.47	13.27(21)	14.98(9)	12.69(20)	15.03(9)
30.02	16.76(3)	17.32(4)	16.29(3)	16.89(4)	69.97	10.90(22)	14.71(11)	10.43(21)	14.78(10)
32.47	16.43(4)	16.98(6)	15.95(4)	16.59(6)	72.47	10.77(18)	14.73(11)	10.29(17)	14.83(11)
34.79	16.31(4)	16.47(7)	15.81(4)	16.16(7)	74.97	11.29(14)	12.74(11)	10.77(13)	12.93(11)
37.47	15.71(5)	16.00(5)	15.20(5)	15.74(5)	77.47	10.88(32)	12.88(11)	10.38(30)	13.08(10)
39.98	15.67(5)	15.72(4)	15.16(5)	15.48(4)	79.97	9.83(15)	13.63(15)	9.38(14)	13.83(15)
42.47	14.72(8)	15.53(6)	14.21(7)	15.34(6)	82.47	9.40(18)	15.08(13)	8.97(17)	15.27(12)
44.97	14.63(8)	15.30(5)	14.11(8)	15.15(4)	84.97	9.60(17)	14.83(6)	9.16(16)	15.05(5)

[a] Values of ΔH^* are obtained from the nonlinear fitting of the expressions for ϵ' and ϵ'' using the Mason et al. (16) and Kaatze (17) values for α and ϵ_∞ and the Vidulich et al. (18) values for $\epsilon_0(t)$.

frequency. Five data points obtained at successive measurement temperatures T_1, T_2, T_3, T_4, and T_5 were used to estimate the values of the parameters at T_3. T_2, T_3, T_4, T_5, and T_6 were then used to estimate the values of the parameters at T_4, etc. The nonlinear analysis used the technique outlined for Press et al. (15). The complete details of the nonlinear fit have been provided by Barajas and Buckmaster (11) and Barajas (12). Parts a and b of Table 3 give the values of ΔH^* calculated from the $\epsilon'(t)$ and $\epsilon''(t)$ data sets for light and heavy water, respectively, assuming the pairs of values of α and ϵ_∞ reported by Mason et al. (16) and Kaatze (17) and the low-frequency temperature dependences of $\epsilon_0(t)$ for light and heavy water reported by Vidulich et al. (18) and given by Hasted (1). Parts a and b of Figure 10 are graphs of the $\Delta H^*_{\epsilon'}$ and $\Delta H^*_{\epsilon''}$ data for light and heavy water, respectively, using the Kaatze values for α and ϵ_∞. Parts a and b of Table 4 give the corresponding values of ΔS^* and parts a and b of Figure 11 are graphs of the $\Delta S^*_{\epsilon'}$ and $\Delta S^*_{\epsilon''}$ data for light and heavy water, respectively, using the Kaatze values for α and ϵ_∞. The values of the standard deviation given in these two tables for light water are much smaller than those reported previously (11). Moreover, the values of $\Delta H^*_{\epsilon'}$ and $\Delta H^*_{\epsilon''}$ and of $\Delta S^*_{\epsilon'}$ and $\Delta S^*_{\epsilon''}$ for light water are in much better agreement than those reported previously (11). This confirms the claim of Barajas and Buckmater (11) that the consistency of these pairs of values can be used as a sensitive diagnostic test to assess the accuracy as well as the precision of a comprehensive complex permittivity data set. These pairs of values are more consistent from approximately 15 to 75 °C, but their 1σ errors do not overlap because of the significant improvement in the 1σ errors for $\Delta H^*_{\epsilon'}$ and $\Delta S^*_{\epsilon'}$ compared to those reported previously (11). This improvement can be ascribed to the use of the Clarke-Hess digital phase meter to determine the values of β.

The temperature dependencies of the Gibbs free energy of activation parameter for the relaxation process (ΔG^*) and the relaxation time (τ) were also calculated using the same methodology outlined by Barajas and Buckmaster (11). Parts a and b of Table 5 give the values of ΔG^* calculated from the values of ΔH^* and ΔS^* given in Tables 3 and 4, respectively, for light and heavy water. Parts a and b of Figure 12 are graphs of the free energy $\Delta G^*_{\epsilon'}$ and $\Delta G^*_{\epsilon''}$ data for light and heavy water, respectively, using the Kaatze (17) values for α and ϵ_∞. Parts a and b of Table 6 give the values of the dielectric relaxation time τ calculated from the values for ΔH^* and ΔS^* given in Tables 3 and 4 for light and heavy water, respectively. Parts a and b of Figure 13 are graphs of this $\tau_{\epsilon'}$ and $\tau_{\epsilon''}$ data for light and heavy water, respectively, using the Kaatze (17) values for α and ϵ_∞. The values of the standard deviation given in these two tables for light water are much smaller and the values of $\Delta G^*_{\epsilon'}$ and $\Delta G^*_{\epsilon''}$ and of $\tau_{\epsilon'}$ and $\tau_{\epsilon''}$ for light water are also in much better agreement than those reported previously (11). The latter are also in good agreement with those reported by Kaatze (17).

The values of $\Delta H^*_{\epsilon''}$ and $\Delta S^*_{\epsilon''}$ are much less reliable than $\Delta H^*_{\epsilon'}$ and $\Delta S^*_{\epsilon'}$ below about 10 °C for both light and heavy water as Figures 10 and 11 reveal. It is concluded

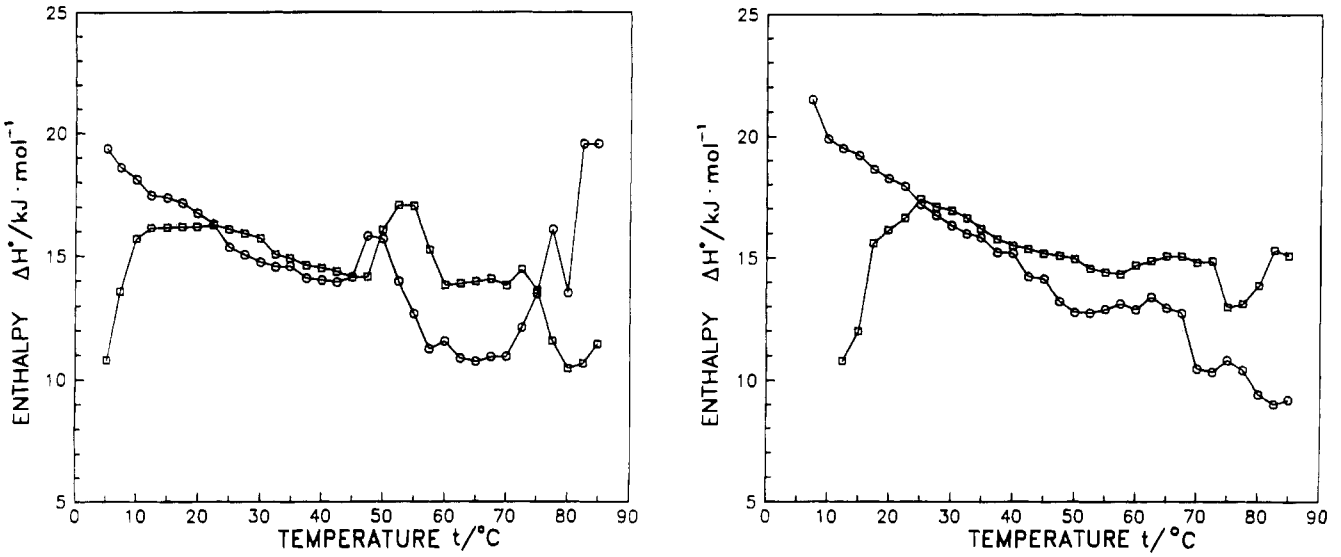

Figure 10. Graphs of the enthalpy of activation $\Delta H^*_{\epsilon'}(t)$ (○) and $\Delta H^*_{\epsilon''}(t)$ (□) as a function of temperature at 9.355 GHz for (a, left) light and (b, right) heavy water using the Kaatze (*17*) values for α and ϵ_∞.

Table 4. Values for the Entropy of Activation ΔS^* and Their Standard Deviations for Double-Distilled, Deionized Water and Heavy Water at 9.355 GHz[a]

	α = 0.013 and ϵ_∞ = 4.25 [from Mason et al. (*16*)]		α = 0 and ϵ_∞ (eq 4) [from Kaatze (*17*)]			α = 0.013 and ϵ_∞ = 4.25 [from Mason et al. (*16*)]		α = 0 and ϵ_∞ (eq 4) [from Kaatze (*17*)]	
t/°C	$\Delta S^*_{\epsilon'}$/ (J·mol^{-1}·K^{-1})	$\Delta S^*_{\epsilon''}$/ (J·mol^{-1}·K^{-1})	$\Delta S^*_{\epsilon'}$/ (J·mol^{-1}·K^{-1})	$\Delta S^*_{\epsilon''}$/ (J·mol^{-1}·K^{-1})	t/°C	$\Delta S^*_{\epsilon'}$/ (J·mol^{-1}·K^{-1})	$\Delta S^*_{\epsilon''}$/ (J·mol^{-1}·K^{-1})	$\Delta S^*_{\epsilon'}$/ (J·mol^{-1}·K^{-1})	$\Delta S^*_{\epsilon''}$/ (J·mol^{-1}·K^{-1})
				(a) Double-Distilled Deionized Water at 5–85 °C					
5.17	33.57(5)	4.11(12)	32.44(5)	2.54(11)	47.49	22.38(24)	15.11(15)	19.74(23)	14.89(14)
7.43	31.04(8)	14.80(11)	29.69(8)	12.38(10)	49.98	22.13(40)	21.13(19)	19.38(38)	20.81(18)
10.07	29.48(7)	21.96(14)	27.97(6)	19.88(13)	52.47	16.59(31)	24.30(13)	14.05(30)	23.98(13)
12.45	27.34(6)	23.17(5)	25.68(6)	21.42(5)	54.97	12.45(41)	24.69(13)	10.08(39)	24.37(12)
15.07	27.06(7)	23.19(5)	25.35(7)	21.46(5)	57.47	7.90(40)	18.34(9)	5.73(38)	18.30(9)
17.47	26.40(11)	23.06(7)	24.63(11)	21.56(7)	59.97	8.97(52)	13.98(13)	6.69(49)	14.09(13)
19.86	25.08(12)	22.79(5)	23.22(11)	21.57(5)	62.47	6.78(30)	14.14(16)	4.57(28)	14.29(15)
22.46	23.57(8)	23.00(5)	21.64(7)	21.80(5)	64.97	6.39(52)	14.28(8)	4.18(49)	14.53(8)
24.99	20.35(9)	22.19(8)	18.41(9)	21.20(8)	67.47	7.06(56)	14.59(8)	4.79(53)	14.84(7)
27.47	19.40(14)	21.54(6)	17.44(14)	20.63(6)	69.97	7.15(40)	13.74(16)	4.80(37)	14.06(16)
30.02	18.45(16)	20.81(5)	16.46(16)	19.97(5)	72.47	10.83(36)	15.52(17)	8.25(33)	15.92(17)
32.47	17.83(18)	18.48(11)	15.81(17)	17.79(10)	74.97	15.18(70)	13.04(9)	12.18(66)	13.53(9)
34.79	18.02(6)	17.90(8)	15.91(6)	17.30(8)	77.47	23.17(64)	6.98(22)	19.63(60)	7.67(22)
37.47	16.49(18)	16.88(10)	14.36(17)	16.36(9)	79.97	15.28(30)	3.63(31)	12.22(28)	4.46(30)
39.98	16.24(20)	16.48(13)	14.09(19)	16.02(12)	82.47	16.91(46)	4.21(22)	33.11(1.0)	5.08(21)
42.47	16.09(27)	15.94(17)	13.86(26)	15.58(16)	84.97	20.04(72)	6.43(21)	33.11(1.7)	7.30(20)
44.97	16.84(22)	15.11(8)	14.55(21)	14.84(8)					
				(b) Heavy Water at 7–85 °C					
7.43	38.50(8)	−4.23(29)	37.74(8)	−79.15(25)	47.49	11.68(16)	16.71(17)	9.82(16)	16.28(16)
10.07	33.19(5)	−24.56(31)	32.05(5)	−56.67(26)	49.98	10.30(25)	16.21(20)	8.45(24)	15.86(19)
12.45	31.89(5)	5.06(13)	30.69(5)	1.14(11)	52.47	10.24(24)	14.86(14)	8.37(23)	14.63(14)
15.07	30.91(5)	9.30(13)	29.64(5)	5.28(10)	54.97	10.77(39)	14.34(11)	8.83(37)	14.18(11)
17.47	29.06(7)	21.06(25)	27.61(7)	17.70(23)	57.47	11.54(34)	14.01(20)	9.53(32)	13.93(19)
19.86	27.82(4)	22.37(20)	26.28(4)	19.53(18)	59.97	10.81(38)	15.09(20)	8.78(36)	15.07(19)
22.46	26.82(8)	23.73(14)	25.17(7)	21.18(13)	62.47	12.53(25)	15.57(11)	10.36(24)	15.60(11)
24.99	24.33(6)	25.96(17)	22.61(6)	23.78(16)	64.97	11.14(45)	16.08(16)	9.00(43)	16.13(16)
27.47	22.88(10)	24.34(21)	21.13(10)	22.68(20)	67.47	10.52(62)	15.98(27)	8.38(58)	16.10(26)
30.02	21.58(9)	23.53(14)	19.79(9)	22.17(13)	69.97	3.56(66)	15.17(31)	1.74(62)	15.38(30)
32.47	20.49(15)	22.44(19)	18.66(14)	21.20(18)	72.47	3.16(54)	15.25(32)	1.35(51)	15.51(31)
34.79	20.07(14)	20.79(24)	18.21(13)	19.81(23)	74.97	4.66(41)	9.49(31)	2.73(38)	10.02(31)
37.47	18.14(16)	19.27(17)	16.22(15)	18.43(17)	77.47	3.51(90)	9.88(30)	1.62(85)	10.45(29)
39.98	18.03(16)	18.35(12)	16.10(15)	17.60(12)	79.97	0.53(42)	12.03(42)	−1.23(40)	12.60(41)
42.47	14.98(24)	17.75(20)	13.07(23)	17.15(19)	82.47	−0.68(49)	16.10(36)	−2.37(46)	16.66(35)
44.97	14.70(26)	17.02(14)	12.76(25)	16.54(14)	84.97	−0.13(48)	15.39(16)	−1.85(45)	16.03(15)

[a] Values of ΔS^* are obtained from the nonlinear fitting of the expressions for ϵ' and ϵ'' using the Mason et al. (*16*) and Kaatze (*17*) values for α and ϵ_∞ and the Vidulich et al. (*18*) values for $\epsilon_0(t)$.

that temperature gradients in the sample make the measured values of α smaller than the true values, and this has a greater effect on the accuracy of $\epsilon''(t)$ then $\epsilon'(t)$ for both light and heavy water in confirmation of the discussion by Barajas and Buckmaster (*11*) for light water. The agreement between the values of $\Delta H^*_{\epsilon'}$ and $\Delta S^*_{\epsilon'}$ above approximately 80 °C is better for heavy than for light water which implies that less bubble formation occurs in the heavy water. This is not surprising since its boiling point is 101.42 °C at sea level and its density is greater than that for light water which lowers the values of $\beta(t)$ and $\epsilon''(t)$ and confirms the analysis given by Barajas and Buckmaster (*11*). Attention is drawn to the unexpected discrepancies between $\Delta G^*_{\epsilon'}$ and $\Delta G^*_{\epsilon''}$ and $\tau_{\epsilon'}$ and $\tau_{\epsilon''}$ below

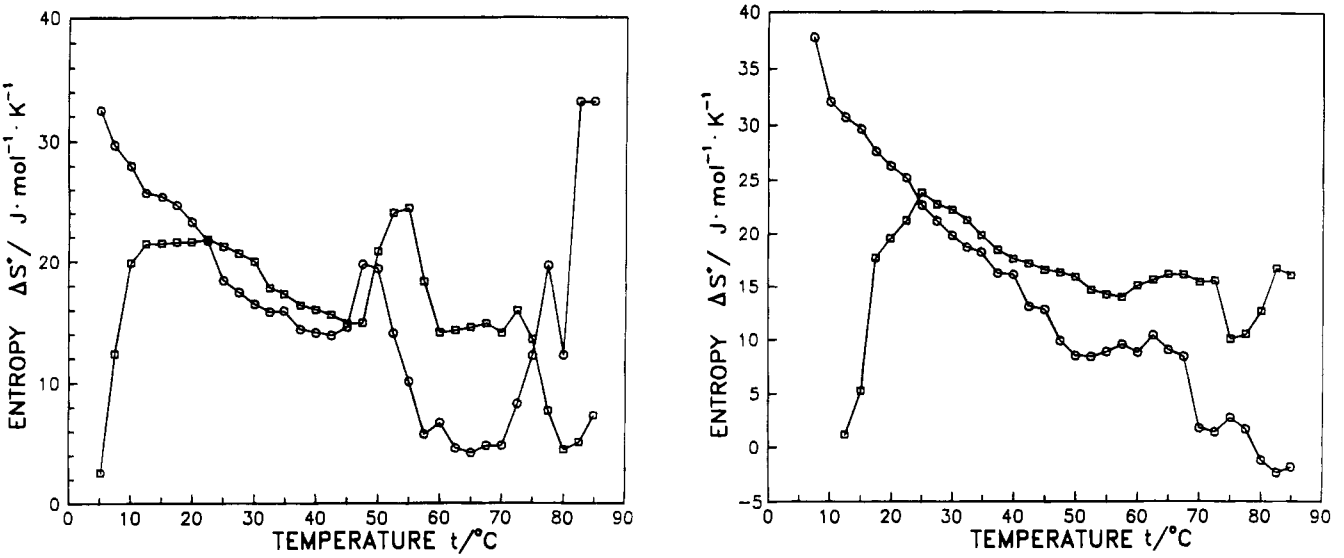

Figure 11. Graphs of the entropy of activation $\Delta S^*_{\epsilon'}(t)$ (○) and $\Delta S^*_{\epsilon''}(t)$ (□) as a function of the temperature at 9.355 GHz for (a, left) light and (b, right) heavy water using the Kaatze (*17*) values for α and ϵ_∞.

Table 5. Values for the Free Energy of Activation ΔG^* and Their Standard Deviations for Double-Distilled, Deionized Water[a] and Heavy Water[b] at 9.355 GHz

	α = 0.013 and ϵ_∞ = 4.25 [from Mason et al. (*16*)]		α = 0 and ϵ_∞ (eq 4) [from Kaatze (*17*)]			α = 0.013 and ϵ_∞ = 4.25 [from Mason et al. (*16*)]		α = 0 and ϵ_∞ (eq 4) [from Kaatze (*17*)]	
t/°C	$\Delta G^*_{\epsilon'}$/ (kJ·mol⁻¹)	$\Delta G^*_{\epsilon''}$/ (kJ·mol⁻¹)	$\Delta G^*_{\epsilon'}$/ (kJ·mol⁻¹)	$\Delta G^*_{\epsilon''}$/ (kJ·mol⁻¹)	*t*/°C	$\Delta G^*_{\epsilon'}$/ (kJ·mol⁻¹)	$\Delta G^*_{\epsilon''}$/ (kJ·mol⁻¹)	$\Delta G^*_{\epsilon'}$/ (kJ·mol⁻¹)	$\Delta G^*_{\epsilon''}$/ (kJ·mol⁻¹)
				(a) Double-Distilled, Deionized Water at 5–85 °C					
5.17	10.29(2)	10.11(5)	10.34(2)	10.09(4)	47.49	9.33(11)	9.35(7)	9.46(11)	9.36(7)
7.43	10.22(3)	10.12(5)	10.26(3)	10.10(4)	49.98	9.29(18)	9.31(9)	9.42(18)	9.32(8)
10.07	10.14(3)	10.09(5)	10.19(3)	10.07(5)	52.47	9.24(14)	9.25(6)	9.38(14)	9.27(6)
12.45	10.07(2)	10.04(2)	10.12(2)	10.02(2)	54.97	9.20(19)	9.19(6)	9.35(18)	9.21(6)
15.07	9.99(3)	9.98(2)	10.06(3)	9.97(2)	57.47	9.17(19)	9.15(4)	9.32(18)	9.17(4)
17.47	9.93(5)	9.92(3)	9.99(4)	9.91(3)	59.97	9.15(24)	9.09(6)	9.31(23)	9.11(6)
19.86	9.87(5)	9.87(2)	9.94(5)	9.86(2)	62.47	9.14(14)	9.06(7)	9.30(13)	9.08(7)
22.46	9.81(3)	9.81(2)	9.89(3)	9.81(2)	64.97	9.12(25)	9.02(4)	9.29(23)	9.04(4)
24.99	9.76(4)	9.75(3)	9.84(4)	9.75(3)	67.47	9.10(27)	8.99(4)	9.27(25)	9.00(4)
27.47	9.70(6)	9.69(3)	9.79(6)	9.70(2)	69.97	9.09(19)	8.95(8)	9.27(18)	8.97(8)
30.02	9.65(7)	9.64(2)	9.74(7)	9.65(2)	72.47	9.06(17)	8.91(8)	9.24(16)	8.93(8)
32.47	9.61(8)	9.59(5)	9.70(8)	9.60(4)	74.97	9.03(35)	8.88(4)	9.22(32)	8.90(4)
34.79	9.57(3)	9.55(4)	9.67(2)	9.56(4)	77.47	8.98(32)	8.85(11)	9.18(30)	8.86(11)
37.47	9.52(8)	9.50(4)	9.62(8)	9.52(4)	79.97	9.96(15)	8.83(15)	9.17(14)	8.84(15)
39.98	9.48(9)	9.46(6)	9.59(9)	9.48(6)	82.47	8.89(23)	8.82(11)	7.76(50)	8.83(11)
42.47	9.44(12)	9.42(8)	9.55(12)	9.44(7)	84.97	8.86(37)	8.80(10)	7.68(85)	8.80(10)
44.97	9.39(10)	9.39(4)	9.51(9)	9.40(4)					
				(b) Heavy Water at 7–85 °C					
7.43	10.87(3)	11.16(11)	10.91(3)	10.26(10)	47.49	9.92(7)	9.84(8)	10.03(7)	9.84(8)
10.07	10.77(2)	11.21(12)	10.81(2)	10.43(10)	49.98	9.89(11)	9.80(9)	10.00(11)	9.80(9)
12.45	10.69(2)	10.51(6)	10.73(2)	10.45(5)	52.47	9.87(11)	9.76(7)	9.98(11)	9.77(6)
15.07	10.61(2)	10.50(5)	10.65(2)	10.45(4)	54.97	9.84(18)	9.73(5)	9.96(17)	9.73(5)
17.47	10.54(3)	10.48(10)	10.59(3)	10.44(10)	57.47	9.81(16)	9.69(9)	9.93(15)	9.70(9)
19.86	10.47(2)	10.43(8)	10.53(2)	10.40(8)	59.97	9.78(18)	9.65(9)	9.91(17)	9.66(9)
22.46	10.40(3)	10.37(6)	10.46(3)	10.34(5)	62.47	9.75(12)	9.62(5)	9.89(12)	9.62(5)
24.99	10.34(3)	10.31(7)	10.40(3)	10.28(7)	64.97	9.72(22)	9.58(8)	9.86(21)	9.58(8)
27.47	10.28(4)	10.24(9)	10.34(4)	10.23(9)	67.47	9.69(30)	9.54(13)	9.84(28)	9.54(12)
30.02	10.22(4)	10.18(6)	10.29(4)	10.17(6)	69.97	9.68(32)	9.50(15)	9.83(30)	9.50(14)
32.47	10.17(6)	10.12(8)	10.25(6)	10.11(8)	72.47	9.68(26)	9.46(15)	9.83(25)	9.47(15)
34.79	10.13(6)	10.07(10)	10.20(6)	10.06(10)	74.97	9.67(20)	9.44(15)	9.82(19)	9.44(15)
37.47	10.08(7)	10.02(8)	10.16(7)	10.02(7)	77.47	9.65(45)	9.41(15)	9.81(42)	9.41(15)
39.98	10.03(7)	9.98(5)	10.12(7)	9.97(5)	79.97	9.65(21)	9.38(21)	9.81(20)	9.38(21)
42.47	9.99(11)	9.93(9)	10.08(10)	9.93(8)	82.47	9.64(25)	9.35(18)	9.81(23)	9.35(17)
44.97	9.95(12)	9.88(7)	10.05(11)	9.89(6)	84.97	9.65(24)	9.31(8)	9.82(23)	9.31(8)

[a] Obtained using the values of ΔH^* and ΔS^* given in Tables 3a and 4a, respectively. [b] Obtained using the values of ΔH^* and ΔS^* given in Tables 3b and 4b, respectively.

10 °C shown in Figures 12b and 13b for heavy water. No satisfactory explanation can be offered except the suggestion that layer effects play a greater role in heavy than in light water which accentuates the temperature gradient effects discussed above. The discrepancies above about 80 °C shown in Figures 12a and 13a for light water are due to the formation of the water vapor bubbles discussed above.

Discussion

The complex permittivity of both light and heavy water are monotonic functions of the temperature as Figure 9

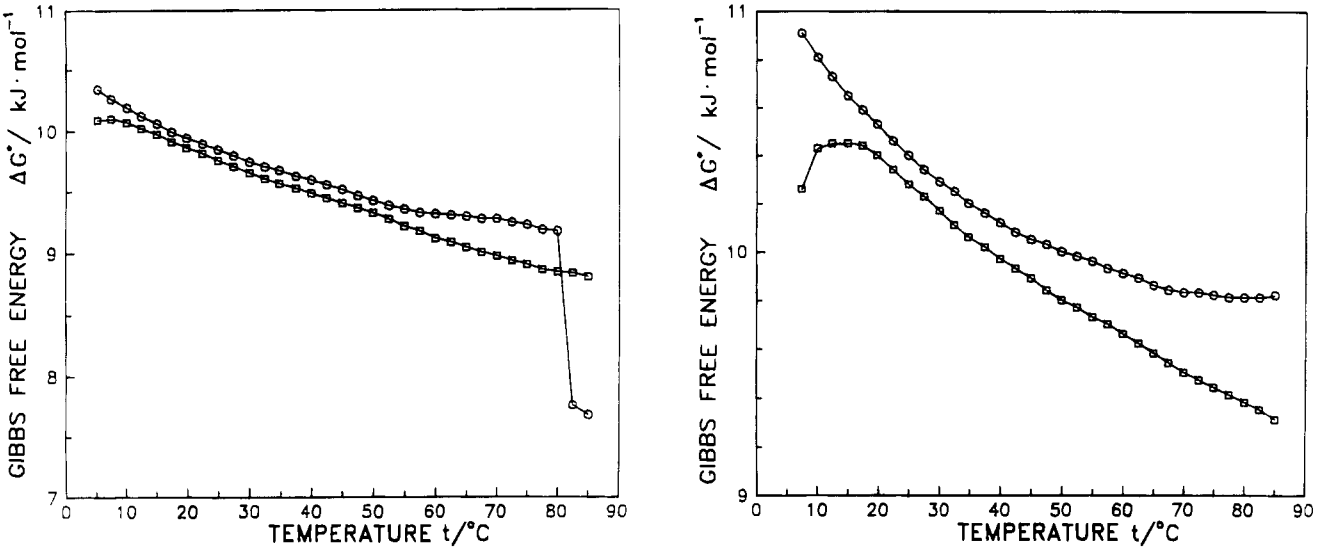

Figure 12. Graphs of the free energy of activation $\Delta G^*_{\epsilon'}(t)$ (○) and $\Delta G^*_{\epsilon''}(t)$ (□) as a function of the temperature at 9.355 GHz for (a, left) light and (b, right) heavy water using the Kaatze (*17*) values for α and ϵ_∞.

Table 6. Values for the Dielectric Relaxation Time τ and Their Standard Deviations for Double-Distilled, Deionized Water[a] and Heavy Water[b] at 9.355 GHz

	α = 0.013 and ϵ_∞ = 4.25 [from Mason et al. (*16*)]		α = 0 and ϵ_∞ (eq 4) [from Kaatze (*17*)]			α = 0.013 and ϵ_∞ = 4.25 [from Mason et al. (*16*)]		α = 0 and ϵ_∞ (eq 4) [from Kaatze (*17*)]	
t/°C	$\tau_{\epsilon'}$/ps	$\tau_{\epsilon''}$/ps	$\tau_{\epsilon'}$/ps	$\tau_{\epsilon''}$/ps	*t*/°C	$\tau_{\epsilon'}$/ps	$\tau_{\epsilon''}$/ps	$\tau_{\epsilon'}$/ps	$\tau_{\epsilon''}$/ps
				(a) Double-Distilled, Deionized Water at 5–85 °C					
5.17	14.71(13)	13.63(28)	15.01(13)	13.48(25)	47.49	4.96(21)	4.99(12)	5.21(21)	5.02(12)
7.43	13.64(18)	13.12(25)	13.93(19)	12.99(23)	49.98	4.71(32)	4.75(15)	4.95(32)	4.78(15)
10.07	12.55(14)	12.30(28)	12.84(14)	12.21(26)	52.47	4.48(24)	4.49(10)	4.72(24)	4.52(10)
12.45	11.65(12)	11.51(10)	11.94(12)	11.44(9)	54.97	4.27(30)	4.24(9)	4.50(30)	4.27(9)
15.07	10.78(13)	10.70(9)	11.06(13)	10.66(8)	57.47	4.08(28)	4.05(6)	4.31(28)	4.08(6)
17.47	10.06(19)	10.02(12)	10.33(19)	10.00(11)	59.97	3.92(34)	3.84(9)	4.16(34)	3.87(9)
19.86	9.41(19)	9.39(9)	9.69(19)	9.39(8)	62.47	3.78(19)	3.67(10)	4.01(19)	3.70(10)
22.46	8.79(11)	8.77(8)	9.07(11)	8.77(8)	64.97	3.64(32)	3.52(5)	3.87(32)	3.54(5)
24.99	8.24(13)	8.22(11)	8.51(13)	8.23(11)	67.47	3.50(33)	3.37(4)	3.72(33)	3.39(4)
27.47	7.75(19)	7.72(8)	8.01(19)	7.74(8)	69.97	3.38(22)	3.22(9)	3.60(22)	3.24(9)
30.02	7.29(20)	7.26(7)	7.55(20)	7.28(7)	72.47	3.25(20)	3.09(9)	3.46(20)	3.11(9)
32.47	6.89(20)	6.85(12)	7.15(21)	6.87(12)	74.97	3.12(37)	2.97(4)	3.34(37)	2.98(4)
34.79	6.54(7)	6.50(9)	6.80(7)	6.53(9)	77.47	2.98(32)	2.85(11)	3.19(33)	2.86(11)
37.47	6.16(19)	6.13(10)	6.41(19)	6.16(10)	79.97	2.88(15)	2.75(14)	3.09(15)	2.76(14)
39.98	5.84(20)	5.81(13)	6.09(20)	5.84(12)	82.47	2.73(21)	2.66(10)	1.86(32)	2.67(10)
42.47	5.54(25)	5.51(16)	5.79(25)	5.55(15)	84.97	2.63(32)	2.57(9)	1.77(50)	2.58(9)
44.97	5.26(19)	5.25(8)	5.50(19)	5.28(7)					
				(b) Heavy Water at 7–85 °C					
7.43	18.10(23)	20.48(1.0)	18.39(23)	13.88(59)	47.49	6.19(17)	6.00(17)	6.44(17)	6.01(17)
10.07	16.44(14)	19.80(1.0)	16.71(14)	14.21(62)	49.98	5.90(25)	5.70(19)	6.14(25)	5.71(19)
12.45	15.16(14)	14.06(32)	15.43(14)	13.71(26)	52.47	5.64(23)	5.43(13)	5.88(23)	5.44(13)
15.07	13.93(12)	13.32(28)	14.19(12)	13.04(23)	54.97	5.39(36)	5.17(10)	5.62(35)	5.18(10)
17.47	12.94(15)	12.65(55)	13.20(15)	12.44(49)	57.47	5.15(29)	4.93(17)	5.39(29)	4.94(16)
19.86	12.06(9)	11.85(39)	12.33(9)	11.69(36)	59.97	4.93(31)	4.70(16)	5.16(31)	4.71(15)
22.46	11.19(14)	11.02(26)	11.44(14)	10.90(24)	62.47	4.71(20)	4.49(8)	4.94(20)	4.49(8)
24.99	10.44(11)	10.29(30)	10.69(11)	10.20(28)	64.97	4.51(35)	4.28(12)	4.73(35)	4.29(11)
27.47	9.76(17)	9.61(34)	10.01(17)	9.55(32)	67.47	4.32(46)	4.09(18)	4.54(45)	4.09(18)
30.02	9.14(14)	8.99(22)	9.40(14)	8.95(20)	69.97	4.17(47)	3.91(20)	4.39(46)	3.91(20)
32.47	8.60(22)	8.44(27)	8.85(21)	8.40(26)	72.47	4.03(36)	3.74(20)	4.24(37)	3.74(20)
34.79	8.14(19)	7.96(33)	8.39(19)	7.94(31)	74.97	3.89(27)	3.59(19)	4.10(27)	3.60(19)
37.47	7.64(20)	7.48(22)	7.89(20)	7.47(21)	77.47	3.75(57)	3.45(18)	3.97(57)	3.45(17)
39.98	7.22(19)	7.07(14)	7.47(19)	7.06(14)	79.97	3.63(26)	3.32(24)	3.84(26)	3.32(23)
42.47	6.84(28)	6.69(22)	7.09(28)	6.69(22)	82.47	3.52(30)	3.19(19)	3.73(30)	3.19(19)
44.97	6.49(28)	6.33(16)	6.74(28)	6.34(15)	84.97	3.42(28)	3.06(8)	3.63(28)	3.06(8)

[a] Obtained using the values of ΔH^* and ΔS^* given in Tables 3a and 4a, respectively. [b] Obtained using the values of ΔH^* and ΔS^* given in Tables 3b and 4b, respectively.

shows. The measurements were made in 2.5 °C steps which are sufficiently small to resolve the discontinuities or "kinks" (*1*) that have been reported at 15(2), 31(3), and 42(3) °C by Drost-Hansen and his co-workers (*19*; see also references therein). Their results were obtained using submicrometer polystyrene suspensions in light water under conditions where the surface area-to-volume ratio was relatively large. The dimensions of the variable-length sample used in this work do not satisfy this condition. Consequently, it can be concluded that no information concerning "vicinal" water can be obtained using the instrumentation system used to make the measurements reported in this paper and described elsewhere (*2*, *10*–*12*). The permittivities of both light and heavy water attain broad maxima centered on 40(1) and 46(1) °C, respectively. It is not surprising that the latter maximum occurs at a

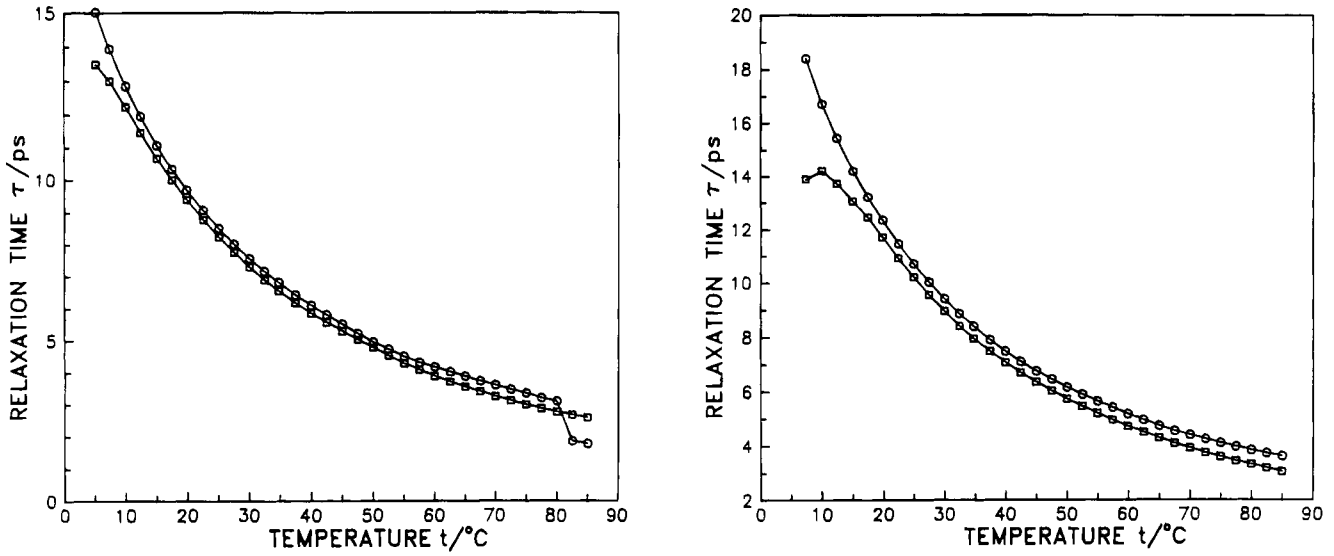

Figure 13. Graphs of the dielectric relaxation time $\tau_{\epsilon'}(t)$ (○) and $\tau_{\epsilon''}(t)$ (□) as a function of the temperature at 9.355 GHz for (a, left) light and (b, right) heavy water using the Kaatze (*17*) values for α and ϵ_∞.

higher temperature than the former because the latter molecule is more massive than the former. Moreover, the maximum density for light water ($d_{max}^{H_2O} = 0.999\ 973$ g/cm^3) occurs at 3.98 °C whereas the maximum density for heavy water ($d_{max}^{D_2O} = 1.106\ 00$ g/cm^3) occurs at 11.185 °C (*20*).

The relaxation times determined using either the Mason et al. (*16*) or the Kaatze (*17*) values for α and ϵ_∞ agree within 5% with previous measurements for both light and heavy water (*14*, *21*, *22*). Table 7 gives the ratio of the relaxation times for heavy and light water reported in Table 6 using the values of $\tau_{\epsilon'}$ and $\tau_{\epsilon''}$ obtained using the Kaatze values for α and ϵ_∞. These ratios should be equal to the ratio of the viscosities of these two liquids (*23*) according to the Debye theory (*1*, *24*). The ratio obtained using ϵ' values agrees with the viscosity ratio to within 2% at temperatures below 50 °C, and the ratio obtained using the ϵ'' values agrees with the viscosity ratio to within 2% at temperatures above 50 °C. The ratio obtained using the ϵ'' values are too small below 20 °C, and those using the ϵ' values are too large above 75 °C. These results confirm the conclusion of Barajas and Buckmaster (*11*) concerning the reliability of the ϵ' and ϵ'' data. It also confirms the validity of the Debye model (*1*, *24*) for the relationship between the relaxation time for the activation process and the viscosity. Some relaxation time ratios reported by Collie et al. (*14*) are also included in Table 7.

The temperature variation parameters for the relaxation process can be interpreted using the above conclusions (*11*). The enthalpy ΔH^* decreases linearly with a slope of approximately −0.14 kJ·mol^{-1}·K^{-1} between 5 °C and 40 °C and is temperature independent with a value of 14 kJ·mol^{-1} from 40 to 85 °C for light water. ΔH^* has a slope of approximately −0.15 kJ·mol^{-1}·K^{-1} between 10 °C and 50 °C and is temperature independent with a value of 14 kJ·mol^{-1} from 50 to 85 °C for heavy water. Similarly the entropy decreases with a slope of −0.46 J·mol^{-1}·K^{-1} between 5 and 40 °C and is temperature independent with a value of 14 J·mol^{-1} from 40 to 85 °C for light water. ΔS^* has a slope of approximately −0.57 J·mol^{-1}·K^{-1} between 5 and 40 °C and is temperature independent with a value of 15 J·mol^{-1} from 40 to 85 °C for heavy water. The values of the slopes are both approximate and subjective. However, they are the best that can be obtained given the experimental problems which limit the accuracy with which the ϵ' and ϵ'' values can be determined. These values for the entropy and enthalpy are in approximate agreement with those estimated using a linear chain model for light water at temperatures below 40 °C (*1*).

Table 7. Ratio of the Relaxation Times for heavy and Light Water at Various Temperatures Calculated from the ϵ' and ϵ'' Data given in Table 6 Assuming α = 0 and the Ratio of the Viscosities for These Liquids at Various Temperatures (*23*)[a]

t/°C	[τD$_2$O/τH$_2$O]$^{\epsilon'}$	[τD$_2$O/τH$_2$O]$^{\epsilon''}$	[ηD$_2$O/ηH$_2$O] (*23*)	[τD$_2$O/τH$_2$O] (*14*)
7.43	1.320	1.069		
10.07	1.301	1.094		1.30
12.45	1.292	1.198		
15.07	1.283	1.223	1.258	
17.47	1.278	1.244		
19.86	1.272	1.245	1.247	1.27
22.46	1.261	1.243		
24.99	1.256	1.239		
27.47	1.250	1.234		
30.02	1.295	1.229	1.228	1.24
32.47	1.238	1.223		
34.79	1.234	1.216		
37.47	1.230	1.213		
39.98	1.227	1.209	1.212	1.19
42.47	1.225	1.205		
44.97	1.225	1.201		
47.49	1.236	1.197		
49.98	1.240	1.195	1.199	
52.47	1.246	1.204		
54.97	1.249	1.213		
57.47	1.250	1.211		
59.97	1.240	1.217	1.188	
62.47	1.232	1.214		
64.97	1.222	1.212		
67.47	1.220	1.206		
69.97	1.219	1.207	1.179	
72.47	1.225	1.203		
74.97	1.228	1.208		
77.47	1.245	1.206		
79.97	1.243	1.203	1.172	
82.47	2.005	1.195		
84.97	2.051	1.186		
90			1.165	

[a] The ratios reported by Collie et al. (*14*) are also included.

Recent work by Mashimo and co-workers (*25*–*28*) using time domain reflectometry has led to the conclusion that light water forms clusters consisting of six molecules whose structure may be hexagonal rings similar to ordinary ice. They studied the effect of the concentration of various water-soluble polymers and organic materials and found that the relaxation time for the mixture always had an

extremum when the molar fraction of water was 0.83 which corresponds to a hexagonal structure consisting of five water molecules and one organic compound molecule. Their conclusion is consistent with that of Ohtomo et al. (*29*) who used neutron diffraction measurements from 20 to 90 °C to show that light water had a crystal-like structure below 40 °C and a liquid-like structure above 40 °C. These results lend credulence to the conclusion that ΔH^* and ΔS^* data obtained from complex permittivity measurements have the potential of being used to test the validity of various models for liquid water.

Summary

This paper has described the recent improvements to the instrumentation system developed to measure the complex permittivity of high loss liquids including light and heavy water using a variable-length transmission sample cell. An error analysis has been attempted for the first time. The results of complex permittivity measurements of heavy water and of double-distilled, deionized light water at 9.355 GHz for the temperature interval from approximately 1 to 90 °C in 2.5 °C increments are given. The former measurements report the first comprehensive, high-precision study for heavy water.

The temperature variation of the activation parameters for the relaxation process has been calculated from both the $\epsilon'(t)$ and $\epsilon''(t)$ data sets for both light and heavy water. The discrepancy between the values obtained from these two sets has been used to confirm and extend the pioneering diagnostic analysis due to Barajas and Buckmaster (*11*). The improved agreement between these values for light water confirms the estimated precision and accuracy has been improved. It has been shown that these improvements lead to uncertainties in the accuracy of $\epsilon'(t)$ and $\epsilon''(t)$ to be approximately ±0.1% for the permittivity and approximately ±0.2% for the dielectric loss and the 1σ precision to be approximately 0.02%. The difference between the accuracy and the precision indicates that further instrumentation system improvements are possible. It is concluded that the temperature variation of the enthalpy and entropy activation parameters for the relaxation process are not sufficiently precise to be used to test the relative validity of the various models for liquid water but that this approach has considerable potential.

Acknowledgment

The assistance and advice of Mr. P. Amerl and the technical support of Dr. J. Kudynska, Mr. C. H. Hansen, Mr. B. Chabot, and Mr. Z. Spevak are gratefully acknowledged.

Literature Cited

(1) Hasted, J. B. *Aqueous Dielectrics*; Chapman and Hall: London, 1973; p 302.
(2) Buckmaster, H. A. *J. Electromagn. Waves Appl.* **1990**, *4*, 645.
(3) McAvoy, J. G.; Buckmaster, H. A. *J. Phys. D: Appl. Phys.* **1983**, *16*, 2519.
(4) McAvoy, J. G.; Buckmaster, H. A. *J. Phys. D: Appl. Phys.* **1984**, *17*, 2081.
(5) McAvoy, J. G.; Buckmaster, H. A. *J. Phys. E: Sci. Instrum.* **1985**, *8*, 244.
(6) Zaghloul, H.; Buckmaster, H. A. *J. Phys. D: Appl. Phys.* **1988**, *18*, 2109.
(7) Buckmaster, H. A.; van Kalleveen, T. H. T.; Zaghloul, H.; Hansen, C. H. *IEEE Trans. Microwave Theory Tech.* **1987**, MTT-35, 909.
(8) Van Kalleveen, T. H. T.; Buckmaster, H. A. *Can J. Chem.* **1988**, *66*, 672.
(9) Buckmaster, H. A.; Hansen, C. H.; van Kalleveen, T. H.T. *IEEE Trans. Instrum. Meas.* **1990**, IM-39, 964.
(10) Buckmaster, H. A. *Trends Microwave Theory Tech.* **1991**, *1*, 87.
(11) Barajas, O.; Buckmaster, H. A. *J. Phys. C: Condens. Matter* **1992**, *4*, 8671.
(12) Barajas, O. Unpublished M.Sc. Thesis, Department of Physics and Astronomy, The University of Calgary, Calgary, Canada, 1992.
(13) Cole, K. S.; Cole, R. H. *J. Chem. Phys.* **1941**, *9*, 341.
(14) Collie, C. H.; Hasted, J. B.; Ritson, D. M. *Proc. Phys. Soc.* **1948**, *60*, 145.
(15) Press, W. H.; Flannery, B. P.; Teukolsky, S. A.; Vetterling, W. T. *Numerical Recipes in C: The Art of Scientific Computing*; Cambridge University Press: New York, 1988; pp 517–565.
(16) Mason, P. R.; Hasted, J. B.; Moore, L. *Adv. Mol. Relax. Processes* **1974**, *6*, 217.
(17) Kaatze, U. *J. Chem. Eng. Data* **1989**, *34*, 371.
(18) Vidulich, G. A.; Evans, D. F.; Kay, R. L. *J. Phys. Chem.* **1967**, *71*, 656.
(19) Drost-Hansen, W.; Singleton, J. L. Our Aqueous Heritage; Evidence for Vicinal Water in Cells, Chapter 5; Chemistry of Living Cell, Vol. 3A. *Fundamentals of Medical Cell Biology*; JAI Press: London, 1991; pp 157–180.
(20) *Handbook of Chemistry and Physics*, 51st ed.; Weast, R. G., Ed.; CRC Press: Cleveland, OH, 1970–71, p F4.
(21) Saxton, J. A. *Proc. R. Soc. London* **1952**, *A213*, 473.
(22) Grant, E. H.; Shack, R. *Br. J. Appl. Phys.* **1967**, *18*, 1807.
(23) Kirillin, V. A. *Heavy Water – Thermophysical Properties*; Israel Program for Scientific Translation: Jerusalem, 1971; p 120, Table 4–8.
(24) Debye, P. *Polar Molecules*; Chemical Catalog Co.: New York, 1929; Chapter V.
(25) Mashimo, S.; Umehara, J.; Redlin, H. *J. Chem. Phys.* **1991**, *95*, 6257.
(26) Mashimo, S.; Miura, N.; Umehara, J.; Yagibara; Higasi, K. *J. Chem. Phys.* **1992**, *96*, 635.
(27) Mashimo, S.; Miura, N.; Umehara, J. *J. Chem. Phys.* **1992**, *97*, 6759.
(28) Miura, N.; Shinyashiki, N.; Mashimo, S. *J. Chem. Phys.* **1992**, *97*, 8722.
(29) Ohtomo, N.; Tokiwano, K.; Arakawa, K. *Bull. Chem. Soc. Jpn.* **1984**, *57*, 329.

Received for review June 28, 1993. Revised February 7, 1994. Accepted May 25, 1994.[⊗] This research was supported by grants awarded by the Natural Sciences and Engineering Research Council of Canada (A-0000716) and The University of Calgary to H.A.B.

[⊗] Abstract published in *Advance ACS Abstracts,* September 1, 1994.